The Influence of Instantons on the Quark Propagator in Lattice Quantum Chromodynamics

Daniel Trewartha

January 2012

A thesis submitted for the degree of Master of Philosophy of the University of Adelaide

THE UNIVERSITY of ADELAIDE

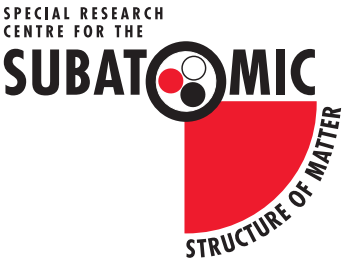

For someone or something or whatever

Declaration

I, Daniel Trewartha, certify that this work contains no material which has been accepted for the award of any other degree or diploma in any university or other tertiary institution and, to the best of my knowledge and belief, contains no material previously published or written by another person, except where due reference has been made in the text.

I give consent to this copy of my thesis, when deposited in the University Library, being made available for loan and photocopying, subject to the provisions of the Copyright Act 1968.

I also give permission for the digital version of my thesis to be made available on the web, via the University's digital research repository, the Library catalogue and also through web search engines, unless permission has been granted by the University to restrict access for a period of time.

Daniel Trewartha Date

Acknowledgements

I'd like to thank my supervisors, Derek Leinweber and Waseem Kamleh, without whose endless patience and advice this thesis would never have happened. I'd also like to thank my family, Hayley and my friends for supporting me for the last two years and dealing stoically with sometimes odd hours and complaints about odder problems.

I could never have lasted two years without conversations both informative and entertaining with my office mates, Adrian, Ben, Nathan, Sam, Sophie and Phiala, who have taught me everything from the finer points of physics to the correct classification of fruits and vegetables.

Those who read parts or all of my thesis helped immensely to make it a far more readable and cogent document than it would otherwise be, and so thanks to Adrian, Andrew, Ben, Brendan and Hayley. Finally I'd like to thank those who either have not been mentioned here at all, or are annoyed they have not been thanked enough. They helped most of all.

Abstract

The non-Abelian nature of quantum chromodynamics means the vacuum cannot be treated as devoid of structure. The non-trivial topology of the vacuum is manifested through instantons, which have important effects on chiral symmetry breaking and dynamical mass generation. We wish to discern the presence and import of instantons on the lattice, first by using the technique of smearing to create lattice configurations which consist solely of instanton-like objects, then calculating the quark propagator on such configurations. Doing so, we hope to understand the role of instantons in the quark propagator.

Contents

List of Figures

Chapter 1

Introduction

During the last century remarkable progress has been made in our understanding of the fundamental mechanisms of the universe. The developments of the two great pillars of modern physics, general relativity and quantum mechanics, lead to a deluge of advancements both theoretical and technological. The most successful scientific theory of all time, the standard model of particle physics, was created in the late 20th century, and continues to be the benchmark for our understanding of reality. Although the standard model has been in existence for over 40 years, it is far from perfectly understood. In particular, quantum chromodynamics (QCD), the portion dealing with the strong interaction, is resistant to normal techniques of solution, and so large questions remain. QCD involves vacuum self-interactions, and thus cannot be treated as empty. This has the effect that at the low energies seen in most matter, QCD is impervious to perturbation theory, and we must perform calculations with other techniques. The lattice, defined in 1974 by Wilson [1], discretises space-time onto a hypercube, allowing us to explicitly solve the QCD governing equations on every space-time point, and extrapolate back to the continuum. Combined with the rapid advances in computing power of the last 30 years, this has proved remarkably successful in solving many problems in QCD. In this thesis we will investigate the influence of instantons, a manifestation of the non-trivial QCD vacuum, on the fundamental fermionic constituents of QCD, the quarks.

We will begin in Chapter (1) with a brief overview of continuum QCD

and the path integral formulation of gauge field theories, along with an introduction to the instanton solution of the Yang-Mills equations. We will then explicitly construct a discretised version of QCD in Chapter (2), before discussing instantons on the lattice, and investigating their properties, in Chapter (3). In Chapter (4) we will define the overlap action, a lattice fermion action with a lattice-deformed chiral symmetry, which will allow us to construct quark propagators with desirable properties for analysis, most notably lack of additive mass renormalisation. Finally in Chapter (5) we will show how to find the non-perturbative quark mass function from these propagators, and present our results.

1.1 Continuum QCD

Quantum Chromodynamics is defined using SU(3) as the gauge group, the group of 3×3 unitary matrices with determinant 1. It thus has Lagrangian density

$$\mathcal{L}_{QCD} = \sum_{i=1}^{\mathrm{N_f}} \bar{\psi}_i (i\not{D} + m_i)\psi_i + \frac{1}{2}\mathrm{Tr} F_{\mu\nu}F^{\mu\nu}, \tag{1.1}$$

which can be decomposed as fermionic and gluonic parts,

$$\mathcal{L}^F_{QCD} = \sum_{i=1}^{\mathrm{N_f}} \bar{\psi}_i (i\not{D} + m_i)\psi_i, \qquad \mathcal{L}^G_{QCD} = \frac{1}{2}\mathrm{Tr}[F_{\mu\nu}F^{\mu\nu}], \tag{1.2}$$

where the fermion fields are summed over the quark flavours. The gluon field A_μ is an element of SU(3), and hence given by

$$A_\mu = \sum_a \lambda^a A^a_\mu, \tag{1.3}$$

with λ^a the generators of the fundamental representation of SU(3).

The covariant derivative D_μ is given by,

$$D_\mu = \partial_\mu + igA_\mu \tag{1.4}$$

and $F_{\mu\nu}$, the field strength tensor, by

$$igF_{\mu\nu} = [D_\mu, D_\nu]. \tag{1.5}$$

g is the QCD coupling constant, whose behaviour as a function of momentum scale Q^2 to first order is given by

$$g^2(Q^2) = \frac{16\pi^2}{(\frac{11}{3}N_c - \frac{2}{3}N_f)\log(Q^2/\Lambda^2_{QCD})}, \tag{1.6}$$

with Λ^2_{QCD} a parameter setting the range at which QCD interactions operate. It is because this coupling constant is near 1 for low Q^2 that QCD remains relatively impervious to the techniques of perturbation theory; higher loop terms remain as large contributions.

Because SU(3) is non-Abelian, it is immediately obvious that eq. (1.2) will give terms cubic and quartic in A_μ. These correspond to gluon self-interactions, and result in a large mass contribution to bound hadronic states, the so-called dynamically generated mass. This is responsible for more than 97% of the mass of the nucleon.

We now investigate the behaviour of A_μ under gauge transformations. The QCD Lagrangian should be invariant under local SU(3) transformations,

$$\psi(x) \to \psi'(x) = G(x)\psi(x) \qquad \bar{\psi}(x) \to \bar{\psi}'(x) = \bar{\psi}(x)G^\dagger(x), \tag{1.7}$$

with $G(x)$ an arbitrary element of SU(3). Inserting into the fermionic part of equation, we find (1.1),

$$\mathcal{L}'_{QCD} = \sum_{i=1}^{\mathrm{N_f}} \bar{\psi}_i G^\dagger(x)(i\not{D}'_\mu + m_i)G(x)\psi_i. \tag{1.8}$$

Thus for gauge invariance, we require

$$\begin{aligned} i\not{D}_\mu &= G^\dagger(x)(\partial_\mu + iA'_\mu)G(x) \\ &= \partial_\mu + G^\dagger(x)(\partial_\mu G(x)) + iG^\dagger(x)A'_\mu G(x), \end{aligned} \tag{1.9}$$

and so we require A_μ to transform as

$$A_\mu \to A'_\mu = G(x)A_\mu G^\dagger(x) + i(\partial G(x))G^\dagger(x). \tag{1.10}$$

It is then trivial to see that the field strength tensor, eq. (1.5), transforms as

$$F_{\mu\nu} \to F'_{\mu\nu} = G(x)F_{\mu\nu}G^\dagger(x). \tag{1.11}$$

The gluonic part of eq. (1.1) transforms as

$$\mathcal{L}^G_{QCD} \to \mathcal{L}'^G_{QCD} = \frac{1}{2}\mathrm{Tr}[G(x)F_{\mu\nu}G^\dagger(x)G(x)F^{\mu\nu}G^\dagger(x)] = \mathcal{L}^G_{QCD} \tag{1.12}$$

using the cyclic property of the trace.

1.2 The Path Integral Formulation

One of the most important developments in 20th century physics was the path integral method for quantum systems. By restoring the connection to the classical action principle lost through canonical quantisation, it opened the gateway to a deeper understanding of gauge field theories, in particular the non-perturbative study of QCD. We present a short overview here, and recommend ref. [9] for in-depth coverage. In order to encode the anti-commuting nature of fermions, we must first define a set of anti-commuting variables, the Grassmann variables.

1.2.1 Grassmann Algebra

The Grassmann algebra generated by n Grassmann numbers $\theta_1, \theta_2, ..., \theta_n$ is the algebra containing the real numbers and the Grassman numbers θ_i, with the defining properties [10]

$$\theta_i\theta_j = -\theta_j\theta_i \quad \forall i,j \in 1,...,n \qquad \theta_i x = x\theta_i \quad \forall x \in \mathbb{R}. \tag{1.13}$$

This has the trivial consequence that

$$\theta_i^2 = 0 \quad \forall i \in 1,...,n. \tag{1.14}$$

Any function on a Grassmann algebra can thus be Taylor expanded as

$$f(\theta) = f_0 + \sum_i f_i\theta_i + \sum_{i\neq j} f_{ij}\theta_i\theta_j + ... + f_{1...n}\theta_1...\theta_n. \tag{1.15}$$

We define an integral on the Grassmann numbers, the Berezin integral, by

$$\int d\theta_i = 0 \tag{1.16}$$

$$\int d\theta_i \, \theta_i = 1 \tag{1.17}$$

noting that the integration measures also anti-commute, i.e.

$$d\theta_i d\theta_j = -d\theta_j d\theta_i \qquad d\theta_i \theta_j = -\theta_j d\theta_i \tag{1.18}$$

Defining a Grassmannian derivative requires somewhat more care. Noting that functions must contain each θ_i as a linear factor or be independent of it, it seems intuitive to define

$$\begin{aligned} \frac{d}{d\theta_i} f(\theta) &= 0 \quad \text{if f is independent of } \theta_i \\ &= 1 \quad \text{otherwise} \end{aligned} \tag{1.19}$$

Cursory examination reveals that this is not well defined; natural numbers commute with Grassmann variables, and we thus have a sign ambiguity. This compels us to require that if f contains θ_i, we must first commute θ_i to the left, and then apply the above.

1.2.2 Path Integral Calculations in QCD

Expressing the fermion fields of QCD as Grassmann variables ψ, we define the partition function of QCD by

$$Z = \int \mathcal{D}\psi \mathcal{D}\bar{\psi} \exp(iS_{QCD}(\psi)). \tag{1.20}$$

We can then calculate vacuum expectation values as

$$\langle \Omega | \psi_1(x) ... \psi_n(x) | \Omega \rangle = \frac{1}{Z} \int \mathcal{D}\psi \mathcal{D}\bar{\psi} \exp(iS_{QCD}(\psi)) \psi_1(x) ... \psi_n(x). \tag{1.21}$$

A problem for numerical simulations is immediately apparent; the weighting factor is given by an imaginary exponential, which is periodic and thus non-trivial to integrate. We can circumvent this by forumlating our simulations in Euclidean space. This can be realised by the transformations

$$x^0 \to -ix_4 \qquad A^0 \to iA_4, \tag{1.22}$$

which gives as action

$$iS^{Minkowski} \to -S^{Euclidean} \tag{1.23}$$

Henceforth $S^{Euclidean}$ shall be referred to simply as S. Then we present without proof the expectation values of observables in QCD as

$$\begin{aligned}\langle \mathrm{O} \rangle &= \frac{1}{Z}\int \mathcal{D}\psi\mathcal{D}\bar{\psi}\mathcal{D}\mathrm{A}\ \mathrm{O}(\psi,\bar{\psi},A)\exp(-S_{QCD}(\psi)) \\ &= \frac{1}{Z}\int \mathcal{D}\mathrm{A}\ \mathrm{O}(\mathrm{D}^{-1},A)\det(\not{D}+m)\exp[-\frac{1}{2}\int d^4x \mathrm{Tr}(F_{\mu\nu}F_{\mu\nu})]\end{aligned} \tag{1.24}$$

where the fermion matrix is defined as $M = \not{D} + m$.

This formulation can then be easily calculated on a given gauge field background. The determinant term provides for quark loops in the vacuum, and is computationally notoriously expensive, and so was set to unity in early calculations. This is known as the quenched approximation, and is equivalent to neglecting sea quark loops. With modern computers, this approximation has been rendered unnecessary, and so we will not use it here.

1.3 Instantons

The non-Abelian nature of SU(3) has more subtle effects on the QCD gauge field than merely allowing gluon self-interactions, creating a rich vacuum topology. The non-trivial topological structure of the QCD vacuum is made manifest through instantons, which carry topological charge. We direct the interested reader to the review [11] for further details of their role in QCD.

We begin our presentation by introducing the general concept of winding number. In the simple case of closed curves in $\mathbb{R}^2\backslash\{0\}$, the winding number around the origin can be intuitively pictured as the number of times the curve wraps around the origin, where anti-clockwise turns are assigned positive winding numbers and clockwise negative. Given the infinitesimal identity in polar coordinates

$$d\theta = \frac{1}{r^2}(x\,dy - y\,dx), \tag{1.25}$$

it is immediately clear we can express the total change in angle of the curve, C, as

$$\delta\theta = \int_C d\theta = \int_C \frac{1}{r^2}(x\,dy - y\,dx), \tag{1.26}$$

and thus the winding number as

$$\text{Winding Number} = \frac{1}{2\pi}\int_C d\theta = \int_C \frac{1}{r^2}(x\,dy - y\,dx). \tag{1.27}$$

We note that as we integrate over a closed curve, the winding number must necessarily be integer valued.

The equivalence classes of curves with equal winding number represent curves that can be continuously deformed into one another without passing through the origin. It is this invariance under homeomorphism that makes the winding number an important topological property. We can generalise this concept to gauge fields, associating an integer winding number, also called the topological charge, to a given gauge configuration. In QCD, we have [11]

$$Q = \frac{g^2}{32\pi^2}\int d^4x \epsilon_{\mu\nu\rho\sigma}\text{Tr}(F_{\mu\nu}(x)F_{\rho\sigma}(x)), \tag{1.28}$$

leading naturally to the definition of the topological charge density, $q(x)$, by

$$Q = \int d^4x\, q(x). \tag{1.29}$$

The first solution with non-trivial topological charge discovered was the (anti-)instanton, with topological charge ± 1. The instanton is a classical solution to the SU(2) Yang-Mills equations, given by [12]

$$A^a_\mu(x,z) = -\frac{2}{g}\frac{\eta_{a\mu\nu}(x-z)_\nu}{(x-z)^2+\rho^2} \tag{1.30}$$

$$A_\mu(x,z) = A^a_\mu\frac{\sigma^a}{2}, \tag{1.31}$$

with ρ the instanton radius, σ the Pauli matrices and $\eta_{a\mu\nu}$ the self-dual 't Hooft symbols [13, 14]. We can write the solution explicitly as

$$A_\mu(x) = \frac{x^2}{x^2+\rho^2}\frac{i}{g}\partial_\mu(S)S^{-1}, \tag{1.32}$$

with S given by

$$S = \frac{x_4 \pm i\vec{x}\cdot\vec{\sigma}}{\sqrt{x^2}}. \tag{1.33}$$

with +/- for instantons/anti-instantons respectively. These provide the only solutions with topological charge ± 1 [16].

We can obtain an SU(3) instanton by embedding the SU(2) solution in one of the SU(2) subgroups of SU(3), typically chosen to be the upper-left 2×2 corner, then performing a rotation to obtain an instanton solution with arbitrary colour orientation. An instanton can be interpreted as a particle existing for an instant, or as a tunneling event between vacuum states which differ by a topological charge of one. They also create exact zero-modes of the Dirac operator, with the sign of the (anti-)instanton prescribing the chirality of the zero-mode [11]. We can link this to the quark condensate via the Banks-Casher relation [17]

$$\langle \overline{q}q \rangle = -\pi \, \rho(0), \text{ as } m_q \to 0, \tag{1.34}$$

with $\rho(0)$ the density of zero modes.

The finite quark condensate has a number of important consequences for QCD, such as dynamical mass generation. Instantons also provide the solution to one of the most intractable problems in QCD, the U(1) problem [18]. Massless QCD has the chiral $\mathrm{U}(1) \otimes \mathrm{SU}(3)$ symmetry at the classical level, which is known to be spontaneously broken in the QCD vacuum by the quark condensate. The U(1) symmetry has corresponding current [19]

$$j^5_\mu = \bar{\psi}(x)\gamma_\mu\gamma_5\psi(x). \tag{1.35}$$

This has no corresponding physical symmetry, and thus should have a massless Goldstone boson. The candidate Goldstone particle however, the η', is far too heavy [20]. This is solved by the non-conservation of the U(1) current by the topological charge density,

$$\partial_\mu j^5_\mu(x) = 2N_f q(x) \tag{1.36}$$

with N_f the number of quark flavours.

This lead to the earliest non-perturbative descriptions of the vacuum as composed of an ensemble of instantons, known as the instanton gas [21]. This features an instanton background made by 'stitching together' instanton solutions at large distances. The model proved unfeasible due to unphysically large instantons dominating, leading to the instanton liquid model [22, 23, 24]. This has much closer spacing, and thus instanton radii are stabilised through interactions [25]. The vacuum is modelled as composed of

equal numbers of instantons and anti-instantons, with equal radius. Phenomenological constraints set the radius to be around $\rho = \frac{1}{3}$fm and density to around $N = 1\text{fm}^{-4}$, with a relatively small packing fraction of $nV_{rminst} = n\frac{\pi^2\rho^4}{2} = \frac{1}{20}$.

Instanton-like objects were found on the lattice as early as 1985 [26], confirming their fundamental importance to QCD. In this thesis we attempt to locate instantons on lattice gauge configurations, quantify their properties and isolate their effects on the quark propagator.

Chapter 2

Constructing QCD on the Lattice

2.1 Discretisation of the Fermion Action

The lattice is defined as an $N_x \times N_y \times N_z \times N_t$ hypercube of volume V and spacings a_x, a_y, a_z, a_t. Here we use a lattice of size $20 \times 20 \times 20 \times 40$, with isotropic spacing $a = 0.126\,\text{fm}$, periodic boundary conditions in space and anti-periodic in time. We restore calculations performed on the lattice to the continuum by taking the limits $a \to 0$ and $V \to \infty$. The lattice discretisation necessarily discretises momentum as

$$P_x = \frac{2\pi}{aN_x} n, \qquad P_t = \frac{2\pi}{aN_t}(n + \frac{1}{2}), \tag{2.1}$$

$$-\frac{N}{2} < n \leq \frac{N}{2}.$$

Discretising the QCD Lagrangian requires somewhat more care than may naively be anticipated; it is important not only that we produce a discrete action with correct continuum limit, but also maintain the vital fundamental properties of QCD such as gauge invariance. We are, however, aided to some extent in that lattice effects of $\mathcal{O}(a)$ or higher are removed in the continuum limit and hence unphysical, and thus we have a certain amount of freedom in choosing discretisations while maintaining the correct continuum limit. We

will often exploit this to create lattice definitions far more complex than the naive discretisation, but which can ensure other desirable properties of the continuum theory are maintained.

We begin with the free fermion action,

$$\mathcal{L}^F_{free} = \sum_{i=1}^{\mathrm{N_f}} \bar{\psi}_i (i\partial\!\!\!/ + m_i)\psi_i. \tag{2.2}$$

The simplest way to discretise this is to replace the derivative with a central difference,

$$\partial\psi(x) \to \frac{1}{2a}(\psi(x+\hat{\mu}) - \psi(x-\hat{\mu})), \tag{2.3}$$

this gives as our first guess for a discretised free fermion action

$$\mathcal{L}^F_{free} = \sum_{i=1}^{\mathrm{N_f}} \bar{\psi}_i \Big[\gamma_\mu \frac{1}{2a}(\psi(x+\hat{\mu}) - \psi(x-\hat{\mu}) + m_i\psi_i)\Big]. \tag{2.4}$$

However, when we consider a gauge transformation, a problem immediately arises.

$$\begin{aligned}
\mathcal{L}'^F_{free} &= \sum_{i=1}^{\mathrm{N_f}} \bar{\psi}_i(x)G^\dagger(x)\Big[\gamma_\mu \frac{1}{2a}(G(x+\hat{\mu})\psi(x+\hat{\mu}) - G(x-\hat{\mu})\psi(x-\hat{\mu}) + m_i G(x)\psi_i(x))\Big] \\
&= \sum_{i=1}^{\mathrm{N_f}} \bar{\psi}_i(x)\Big[\gamma_\mu \frac{1}{2a}(G^\dagger(x)G(x+\hat{\mu})\psi(x+\hat{\mu}) - G^\dagger(x)G(x-\hat{\mu})\psi(x-\hat{\mu}) + m_i\psi_i(x))\Big] \\
&\neq \mathcal{L}^F_{free}.
\end{aligned} \tag{2.5}$$

The origin of the problem is apparent; although ψ lives in a different vector space for each x, we have merely shifted $\psi(x) \to \psi(x+a)$ without consideration of this. It is clear we must discretise the parallel transport operator to compare appropriately.

In the continuum the parallel transporter, commonly known as the Wilson line, transporting $\psi(x) \to \psi(y)$ along curve C is given by

$$U(y,x) = \mathcal{P}\exp(ig\int_C A_\mu dx^\mu). \tag{2.6}$$

We are interested only in C a straight line of length a, and so discretising this, we obtain the lattice parallel transport operator, known as the gauge link;

$$U_\mu(x) = \exp(igaA_\mu(x)). \tag{2.7}$$

We also define T_μ by

$$T_\mu \psi(x) = U_\mu(x)\psi(x+\hat{\mu}) \qquad T_\mu^\dagger \psi(x) = U_\mu^\dagger(x)\psi(x-\hat{\mu}) \tag{2.8}$$

From this we can see that the gauge fields are discretised onto links between lattice sites; their interactions with the fermion fields are through the parallel transport operators.

It is immediately clear that the parallel transport operators transform as

$$U_\mu(x) \to U'_\mu(x) = G(x)U_\mu(x)G^\dagger(x+\hat{\mu}). \tag{2.9}$$

We can thus define a lattice central difference operator,

$$\nabla_\mu = \frac{1}{2a}(T_\mu(x) - T_\mu^\dagger(x)), \tag{2.10}$$

and using this in eq. (2.4), we obtain

$$\mathcal{L}^F_{free} = \sum_{i=1}^{\mathrm{N_f}} \bar{\psi}_i(x)(\gamma^\mu \nabla_\mu + m)\psi_i(x). \tag{2.11}$$

Noting that the parallel transport operators can be Taylor expanded as

$$U_\mu(x) = 1 + iagA_\mu(x) + \mathcal{O}(a^2), \tag{2.12}$$

we can then expand eq. (2.11) as

$$\begin{aligned} \mathcal{L}^F_{free} &= \sum_{i=1}^{\mathrm{N_f}} \bar{\psi}_i(x)(\gamma^\mu \frac{1}{2a}(T_\mu(x) - T_\mu^\dagger(x)) + m)\psi_i(x) \\ &= \sum_{i=1}^{\mathrm{N_f}} \bar{\psi}_i(x)\Big[\gamma_\mu \frac{1}{2a}(\psi(x+\hat{\mu}) - \psi(x-\hat{\mu}) + m_i\psi_i(x) + g\gamma_\mu A_\mu(x)\psi(x)\Big], \end{aligned} \tag{2.13}$$

which includes the desired gauge field interactions, and so the correct continuum limit is maintained.

This is the simplest working definition of a discretised fermion field under the influence of a gauge field. Creating a usable fermion action involves solving some additional complications, which will be dealt with in chapter (4).

2.2 Discretisation of the Gluon Action

It is now possible to discretise the gluon action, realising we must work with U_μ. Examining eq. (2.9), it is obvious that the trace of a closed loop will be gauge invariant, as the cyclic property will allow us to cancel gauge terms appropriately. The simplest closed loop is a 1×1 square, known as the plaquette, given by

$$P_{\mu\nu}(x) = U_\mu(x)U_\nu(x+\hat{\mu})U_\mu^\dagger(x+\hat{\nu})U_\nu^\dagger(x). \tag{2.14}$$

Thus equipped with a tool for defining gluon fields on the lattice, we can define the Wilson gauge action using a sum over all plaquettes touching a point,

$$\mathcal{S}^G = \frac{g}{g^2}\sum_x \sum_{\mu<\nu} \frac{1}{3}\mathrm{ReTr}[1 - P_{\mu\nu}(x)], \tag{2.15}$$

noting that the integral has been discretised with a sum over x, and we sum over $\mu < \nu$ to avoid double counting.

To verify this gives the correct continuum limit, we expand gauge links using eq. (2.7), noting that due to the non-Abelian nature of the gauge field it is necessary to use the Baker-Campbell-Hausdorff formula for exponentials,

$$\exp(aA)\exp(aB) = exp\Big(aA + aB + \frac{a^2}{2}[A,B] + \mathcal{O}(a^3)\Big), \tag{2.16}$$

giving

$$\begin{aligned} P_{\mu\nu}(x) &= \exp\Big(igaA_\mu(x)\exp(igaA_\nu(x+\hat{\mu}))\exp(-igaA_\mu(x+\hat{\nu}))\exp(-igaA_\nu(x)\Big) \\ &= \exp\Big(igaA_\mu(x) + igaA_\nu(x+\hat{\mu}) - \frac{g^2a^2}{2}[A_\mu(x), A_\nu(x+\hat{\mu})] - igaA_\mu(x+\hat{\nu}) \\ &- igaA_\nu(x) - \frac{g^2a^2}{2}[A_\mu(x+\hat{\nu}), A_\nu(x)] + \frac{g^2a^2}{2}[A_\nu(x+\hat{\mu}), A_\mu(x+\hat{\nu})] \\ &+ \frac{g^2a^2}{2}[A_\mu(x), A_\nu(x)] + \frac{g^2a^2}{2}[A_\mu(x), A_\mu(x+\hat{\nu})] + \frac{g^2a^2}{2}[A_\nu(x+\hat{\mu}), A_\nu(x)] + \mathcal{O}(a^3)\Big) \end{aligned} \tag{2.17}$$

For simplicity, we then Taylor expand shifted terms in terms of the field at x, i.e.

$$A_\mu(x+\hat{\mu}) = A_\mu(x) + a\partial_\mu A_\mu(x). \tag{2.18}$$

Expanding and cancelling terms, we acquire

$$\begin{aligned} P_{\mu\nu}(x) &= \exp\Big(ig^2a^2(\partial_\mu A_\nu(x) - \partial_\nu A_\mu(x) + ig[A_\mu(x), A_\nu(x)] + \mathcal{O}(a^3)\Big) \\ &= \exp\Big(ig^2a^2F_{\mu\nu}(x) + \mathcal{O}(a^3)\Big) \\ &= 1 + ig^2a^2F_{\mu\nu}(x) - \frac{g^4a^4F_{\mu\nu}^2(x)}{2} - \frac{ig^6a^6F_{\mu\nu}^3(x)}{6} + \mathcal{O}(a^8). \quad (2.19) \end{aligned}$$

Before inserting this into the Wilson action, we note that

$$\mathrm{ReTr}[U_{\mu\nu}(x)] = \mathrm{ReTr}[U_{\mu\nu}(x)]^* = \mathrm{ReTr}[U_{\mu\nu}^\dagger(x)] = \mathrm{ReTr}[U_{\nu\mu}(x)], \quad (2.20)$$

and so only terms symmetric in μ, ν will survive. This implies that terms with an even power of $F_{\mu\nu}$ remain, and we can simplify the sum as $\sum_{\mu<\nu} = \frac{1}{2}\sum_{\mu,\nu}$. Using this in eq. (2.15), we find

$$\mathcal{S}^G = \frac{a^4}{2}\sum_x\sum_{\mu,\nu}\mathrm{Tr}[F_{\mu\nu}(x)^2], \quad (2.21)$$

which has the correct continuum limit.

2.3 Improved Gluon Actions

The Wilson gauge action, while having the advantage of being relatively simple, is not the only choice of action. Noting that unitarity of the links implies that $P_{\mu\nu}^\dagger = P_{\mu\nu}^{-1}$ is the plaquette in the opposite direction to $P_{\mu\nu}$, we can average over clockwise and anti-clockwise plaquettes to obtain

$$\mathcal{S}^G = \frac{2}{g^2}\sum_x\sum_{\mu,\nu}\mathrm{Tr}[1 - \frac{1}{2}(P_{\mu\nu}(x) + P_{\mu\nu}^\dagger(x))]. \quad (2.22)$$

We also note that terms of higher order than a^4 will vanish in the continuum limit, and so can be added freely [2]. This implies that by building an action out of loops more complex than plaquettes, we can choose coefficients to minimise the error terms. Given the 2×1 loop,

$$R_{\mu\nu}(x) = U_\mu(x)U_\nu(x+\hat{\mu})U_\nu(x+\hat{\nu}+\hat{\mu})U_\mu^\dagger(x+2\hat{\nu})U_\nu^\dagger(x+\hat{\nu})U_\nu^\dagger(x) + \text{Hermitian conjugate}, \quad (2.23)$$

we can define a gauge action by simply replacing plaquettes in (2.15). This action has different $\mathcal{O}(a^6)$ errors, and so by summing the two actions with appropriate coefficients, these can be eliminated. The result is the Symanzik improved action [2];

$$\mathcal{S}^G_{Symanzik} = \frac{10}{3g^2}\sum_x \mathrm{Tr}[1-\frac{1}{2}(P_{\mu\nu}(x)+P^\dagger_{\mu\nu}(x))]-\frac{1}{6g^2}\mathrm{Tr}[1-\frac{1}{2}(R_{\mu\nu}(x)+R^\dagger_{\mu\nu}(x))]. \tag{2.24}$$

Even this improved action however, generates relatively poor agreement with perturbation theory in high energy regions, initially casting doubt on the veracity of lattice non-perturbative calculations. This issue was solved by Lepage and MacKenzie [4], who noted that although higher order terms in the Taylor expansion of the parallel transport operators(2.12) appear to be suppressed by higher powers of a, contracted factors of A_μ generate ultra-violet divergences which precisely cancel factors of a. This means that higher order terms are in fact only suppressed by powers of g, which are close to 1 in the regions in which we are interested. Although we naively expect that the vacuum expecation value of the parallel transport operator will be similar to the continuum result,

$$\langle 1 + iagA_\mu\rangle \approx 1 \approx \langle U_\mu(x)\rangle, \tag{2.25}$$

these large higher order terms act to renormalise it away from 1. A simple solution immediately presents itself; if we define a scalar u_0, the mean field improvement factor, that normalises the gauge links appropriately we can define the mean field improved link,

$$U^{\mathrm{mfi}}_\mu(x) = \frac{U_\mu(x)}{u_0}, \tag{2.26}$$

which should have the appropriate vacuum expectation value.

u_0 is calculated non-perturbatively. The definition is not unique, here we use

$$u_0 =< \frac{1}{3}\mathrm{Tr}P_{\mu\nu}(x) >^{\frac{1}{4}} . \tag{2.27}$$

We note that in the continuum limit $u_0 \to 1$, and so the correct continuum limit is maintained.

The use of u_0 is only approximate, and values much diverged from 1 will result in large errors, particularly if higher powers of u_0 are used.

2.4 Gauge Fixing on the Lattice

We are primarily interested in calculating the gauge-dependent quark propagator, and so must gauge fix in order to produce useful results. For reasons of simplicity and ease of comparison to other studies, we choose to fix to Landau gauge, defined in the continuum by

$$\partial_\mu A_\mu(x) = 0. \tag{2.28}$$

This prescription cannot be naively discretised; on the lattice gauge fields are contained in the link variables, which are SU(3) valued and so do not have a derivative. We must therefore find an alternative expression for the gauge fixing condition, which we can then discretise. Consider the functional of the gauge field [5], $\mathcal{F}(G)$,

$$\mathcal{F}(G) = \int \mathrm{d}^4x \mathrm{Tr}[A^G_\mu(x)^2]. \tag{2.29}$$

We examine the effect of small gauge changes by parameterising an infinitesimal gauge transformation as

$$G(x) = \exp(-i\epsilon H(x)) \tag{2.30}$$

and inserting into the gauge transformation of A_μ, eq. (1.10). We find that it transforms as

$$\begin{aligned} A_\mu(x) \to A'_\mu(x) &= G(x)A_\mu G^\dagger(x) + i(\partial G(x))G^\dagger(x) \\ &= \exp(-i\epsilon H(x))A_\mu \exp(i\epsilon H(x)) + i(\partial \exp(-i\epsilon H(x))) \exp(i\epsilon H(x)) \\ &= A_\mu(x) + i\epsilon[H(x), A_\mu(x)] + i(\partial(1 - i\epsilon H(x)))(1 + i\epsilon H(x)) + \mathcal{O}(\epsilon^2) \\ &= A_\mu(x) + \epsilon\Big(i[H(x), A_\mu(x)] - \partial H(x)\Big) + \mathcal{O}(\epsilon^2). \end{aligned} \tag{2.31}$$

Substituting this into eq. (2.29), we find

$$\mathcal{F}(G) \to \mathcal{F}(G) - 2\epsilon \int \mathrm{d}^4x \mathrm{Tr}[A_\mu(x)\partial H(x)] + \epsilon^2. \tag{2.32}$$

Performing an integration by parts and discarding surface terms,

$$= \mathcal{F}(G) + 2\epsilon \int \mathrm{d}^4x \mathrm{Tr}[(\partial A_\mu(x))H(x)] + \epsilon^2. \tag{2.33}$$

From this we see that if $\mathcal{F}(G)$ is at an extremum, $\mathcal{O}(\epsilon)$ terms must vanish. Since $H(x)$ is arbitrary, this implies that $\partial_\mu A_\mu = 0$, and so finding a extrema of eq. (2.29) is equivalent to finding solutions of eq. (2.28). This formulation can easily be discretised, it is clear that the lattice equivalent is

$$\mathcal{F}(G) = a^2 \sum_x \sum_{\mu=1}^{4} \mathrm{Tr}(U_\mu(x) + U_\mu^\dagger(x)). \tag{2.34}$$

We can then use numerical methods to find a gauge transformation minimising this on our configurations.

2.5 Discretisation of the Field Strength Tensor

We have until now been discretising $F_{\mu\nu}(x)$ merely by replacing continuum covariant derivatives with their lattice equivalents. This has allowed us to construct a simple lattice gluonic action. However when we use it directly, it is desirable to have a definition that is closer to its continuum counterpart. If we set the lattice $F_{\mu\nu}(x)$ to the solution of

$$[\nabla_\mu(x), \nabla_\nu(x)]\psi(x) = igF_{\mu\nu}(x)\psi(x) \tag{2.35}$$

we can expect a better result.

One solution is the clover improved field strength tensor,

$$F_{\mu\nu}^{cl}(x) = \frac{1}{2iga^2}[C_{\mu\nu}(x) - C_{\mu\nu}^\dagger(x)], \tag{2.36}$$

with $C_{\mu\nu}(x)$ the clover term,

$$C_{\mu\nu}(x) = \frac{1}{4}[U_{\mu\nu}(x) + U_{\mu-\nu}(x) + U_{-\mu-\nu}(x) + U_{-\mu\nu}(x)]. \tag{2.37}$$

This is identical to the naively discretised $F_{\mu\nu}(x)$ up to $\mathcal{O}(a^2)$. Our experience with improving the gluonic action suggests we can reduce errors further by choosing combinations of larger loops carefully. Defining the $m \times n$ clover $C_{\mu\nu}^{m\times n}(x)$ as the sum of the four $m \times n$ loops starting at x in the $\hat{\mu}\hat{\nu}$ plane,

we define a general improved field strength tensor as [38]

$$F^{\text{imp}}_{\mu\nu}(x) = k_1 F^{1\times1}_{\mu\nu}(x)+k_2 F^{2\times2}_{\mu\nu}(x)+k_3 F^{2\times1}_{\mu\nu}(x)+k_4 F^{3\times1}_{\mu\nu}(x)+k_5 F^{3\times2}_{\mu\nu}(x)+k_6 F^{3\times3}_{\mu\nu}(x). \tag{2.38}$$

Expanding this in powers of a and demanding that $\mathcal{O}(a^2)$ and $\mathcal{O}(a^4)$ terms vanish, we acquire a set of equations in the parameters k_i. The solution with minimal $k_i \neq 0$, and thus the most computationally efficient, is given by [6]

$$F^{\text{imp}}_{\mu\nu}(x) = \frac{3}{2u_0^4} F^{1\times1}_{\mu\nu}(x) - \frac{3}{20u_0^8} F^{2\times2}_{\mu\nu}(x) + \frac{1}{90u_0^{12}} F^{3\times3}_{\mu\nu}(x). \tag{2.39}$$

Some care must be taken in using this definition; it includes factors of u_0^{12} which are highly dependent on fluctuations in the gauge field, and so we must dampen short-range effects before we can be confident of its accuracy.

2.6 Discretisation of the Topological Charge Density

To define a lattice topological charge density operator, we can easily imagine discretising eq. (1.28). One possibility with correct continuum limit is [7]

$$q(x) = \frac{g^2}{16\pi^2} \text{Tr}[\epsilon^{\mu\nu\rho\sigma} F_{\mu\nu}(x) F_{\rho\sigma}(x)], \tag{2.40}$$

which allows us to then define the overall topological charge as

$$Q = \sum_x q(x). \tag{2.41}$$

This quickly runs into seemingly insurmountable problems; the topological charge is non-integer valued, as the topological charge density is overly affected by short-range behaviour of order a [8]. Although we may naively expect these gluon field fluctuations to vanish as we take the continuum limit, they in fact become divergent. This suggests that in order to have a meaningful definition of the lattice topological charge, we must first remove short-range fluctuations, leaving only the long-range effects which in the continuum are responsible for a non-trivial topological charge.

Chapter 3

Cooling and Smearing

3.1 Cooling and Smearing algorithms

In the study of lattice QCD, it is often desirable to suppress quantum fluctuations, as these short-range effects can obscure long distance physics. In particular, here we wish to isolate instanton effects, requiring suppression of UV noise. In order to deal with this problem, we seek to remove fluctuations away from the classical solution to the gauge action. As instantons are solutions to the classical equations of motion, these should survive, while fluctuations in the action due merely to quantum effects should be removed. This suspicion was first confirmed in [15], which found instanton-like objects on the lattice using this technique. The procedure is known as cooling, and was first applied to the O(3) sigma model [26, 27, 28]. Roughly speaking, it consists of systematically sweeping all links $U_\mu(x)$ and replacing them with a new link, $U'_\mu(x)$ such that the gluonic action is minimised for that link. It is convenient to first write the local Wilson action as a function of $U_\mu(x)$

$$S_W = \frac{2}{g^2} \sum_{\mu<\nu} \mathrm{ReTr}[1 - U_\mu(x)\Xi_{\mu\nu}(x)], \tag{3.1}$$

where we have defined $\Xi_{\mu\nu}(x)$ as the sum of the two 'staples' of three links in $P_{\mu\nu}(x)$ not including $U_\mu(x)$ lying in the $\mu\nu$ plane. Thus our new link should be chosen to maximise

$$\mathrm{ReTr}[U_\mu(x) \sum_{\mu<\nu} \Xi_{\mu\nu}(x)]. \tag{3.2}$$

Cooling removes action from the gauge field quickly, however the $\Xi_{\mu\nu}(x)$ terms contain other links, and so when updating in parallel links which are contained in the local action of a neighbouring link cannot be changed. This makes standard cooling a poor algorithm in practical application, and so other algorithms are commonly used.

These include APE smearing [30], whereby all links are simultaneously updated by averaging with neighbouring links, and so

$$U'_\mu(x) = (1-\alpha)U_\mu(x) + \frac{\alpha}{6}\sum_{\nu\neq\mu}\Xi^\dagger_{\mu\nu}(x), \tag{3.3}$$

where α is a real parameter governing the extent to which we 'smear' links. However addition is not an SU(3) operation, so it is necessary to project the result back onto an SU(3) element. This projection operation is not uniquely defined, and must be performed carefully so as to maintain physical symmetries to the greatest possible extent. This also requires the use of a branch cut, and thus removing differentiability. For these reasons, APE smearing is somewhat undesirable for use in practice, though its development lead to new forms of smearing, which we will later examine.

Although it is not immediately obvious that this step serves to reduce the action toward the classical solution in the same way cooling does, it is intuitively clear. Noise is by nature a local effect, and so by taking a (weighted) average as above the links are reduced toward the underlying trend. This can be seen clearly using the most common choice of projection step,

$$\mathrm{MaxReTr}(U_\mu(x)U^{'\dagger}_\mu(x)) = \mathrm{MaxReTr}((1-\alpha)U^2_\mu(x) + \frac{\alpha}{6}\sum_{\nu\neq\mu}\Xi^\dagger_{\mu\nu}(x)), \tag{3.4}$$

whereby it is clear that cooling and APE smearing are equivalent for $\alpha = 1$, and so cooling can be viewed as the limit whereby the links are updated sequentially. Indeed, empirical studies have shown gauge fields generated from cooling and smearing to be similar [33].

To avoid the problematic projection step, it is possible to use the exponential function instead of an additive step. From the Taylor expansion, it is clear that to first order this is equivalent, and as the exponential is an SU(3) operation the projection step is unnecessary. This is known as stout

link smearing [31]. Explicitly, stout link smearing uses a weighted sum of staples, similar to the definition of $\Xi_{\mu\nu}(x)$ above,

$$C_\mu(x) = \rho_{\mu\nu}(x)\Xi_{\mu\nu}(x), \tag{3.5}$$

where $\rho_{\mu\nu}$ are the weights, noting there is no sum over μ. To ensure spatial symmetry, ρ_{jk} are taken to be equal. Then we define

$$\Omega_\mu(x) = C_\mu(x)U_\mu^\dagger(x) \tag{3.6}$$

and thus

$$Q_\mu(x) = \frac{i}{2}(\Omega_\mu^\dagger(x) - \Omega_\mu(x)) - \frac{i}{2N}\mathrm{Tr}(\Omega_\mu^\dagger(x) - \Omega_\mu(x)). \tag{3.7}$$

$Q_\mu(x)$ is Hermitian and traceless, and so its exponential is in SU(3). Now we can define the smeared link as

$$U'_\mu(x) = \exp(iQ_\mu(x))U_\mu(x) \tag{3.8}$$

noting for the case of isotropic weights(ie $\rho_{\mu\nu} = \rho$ is constant) this is equivalent to APE smearing to first order.

Since stout link smearing forms the basis for the smearing used in this thesis, we will take the time to show some desirable properties shared by it and its derivative smearing techniques. First, we will explicitly check behaviour under symmetries. We begin with checking local gauge symmetries, following the chain of definitions, beginning with $C_\mu(x)$

$$\begin{aligned} C_\mu(x) \to C'_\mu(x) &= \rho_{\mu\nu}\sum_{\nu\neq\mu}(G(x)U_\nu(x)G^\dagger(x+\hat{\nu})G(x+\hat{\nu})U_\mu(x+\hat{\nu})G^\dagger(x+\hat{\nu}+\hat{\mu}) \\ &\quad G(x+\hat{\nu}+\hat{\mu})U_\nu^\dagger(x+\hat{\mu})G^\dagger(x+\hat{\mu}) + G(x+\hat{\nu}-\hat{\nu})U_\nu^\dagger(x-\hat{\nu}) \\ &\quad G^\dagger(x-\hat{\nu})G(x-\hat{\nu})U_\mu(x-\hat{\nu})G^\dagger(x-\hat{\nu}+\hat{\mu})G(x-\hat{\nu}+\hat{\mu}) \\ &\quad U_\nu(x-\hat{\nu}+\hat{\mu})G(x-\hat{\nu}+\hat{\mu}+\hat{\nu}) \\ &= G(x)C_\mu(x)G(x+\hat{\mu}) \end{aligned} \tag{3.9}$$

then,

$$\begin{aligned} \Omega_\mu(x) \to \Omega'_\mu(x) &= G(x)C_\mu(x)G(x+\hat{\mu})G^\dagger(x+\hat{\mu})U_\mu^\dagger(x)G^\dagger(x) \\ &= G(x)\Omega_\mu(x)G^\dagger(x) \end{aligned} \tag{3.10}$$

$$Q_\mu(x) \to Q'_\mu(x) = G(x)Q_\mu(x)G^\dagger(x). \tag{3.11}$$

Using the Hermitian and traceless properties of $Q_\mu(x)$,

$$\exp(iQ_\mu(x)) \to G(x)\exp(iQ_\mu(x))G^\dagger(x). \tag{3.12}$$

Finally we can insert this into the definition of the smeared link, obtaining

$$U'_\mu(x) \to G(x)\exp(iQ_\mu(x))G^\dagger(x)G(x)U_\mu(x)G^\dagger(x+\hat{\mu}) = G(x)U'_\mu(x)G^\dagger(x+\hat{\mu}). \tag{3.13}$$

Thus the stout link smeared links transform appropriately under local gauge transformations.

Clearly, given a reasonable choice of $\rho_{\mu\nu}$, the smeared link obeys rotation invariance, and reflection in a plane containing the link. For reflection in a plane normal to the link, through the midpoint $x + \frac{1}{2}\hat{\mu}$,

$$\begin{aligned} U_\mu(x) &\to U_{-\mu}(x+\hat{\mu}) = U^\dagger_\mu(x) \\ U_\nu(x) &\to U_\nu(x+\hat{\mu}), \end{aligned} \tag{3.14}$$

and so,

$$\begin{aligned} C_\mu(x) &\to C^\dagger_\mu(x) \\ \Omega_\mu(x) &\to C^\dagger_\mu(x)U_\mu(x) = U^\dagger_\mu(x)\Omega^\dagger_\mu(x)U_\mu(x) \\ Q_\mu(x) &\to -U^\dagger_\mu(x)Q_\mu(x)U_\mu(x) \\ U'_\mu &\to U^\dagger_\mu(x)\exp(iQ_\mu(x)) = U'^\dagger_\mu \end{aligned} \tag{3.15}$$

as required.

Translational symmetries are obvious given $\rho_{\mu\nu}$ is location independent. Thus the smeared link shares with the original link all symmetries.

It is possible to define other smearing algorithms by changing the paths summed over in $C_\mu(x)$, such as in HYP [32] smearing, however as we will be using standard stout link smearing, these will not be discussed here.

Having now seen common smearing algorithms, we will explore the behaviour of instantons under cooling and smearing.

3.2 Behaviour of Instantons under Cooling and Smearing

Although it may be naively expected that cooling algorithms should make instantons more visible, it was observed as early as their discovery on the lattice that successive sweeps of cooling can make instantons, particularly smaller ones, reduce in size and eventually 'fall through' the lattice [35]. To understand this behaviour, we substitute into the Wilson gauge action the single instanton solution in the continuum eq. (1.32). Although this is a continuum solution, we can substitute it on the lattice given $\rho_{inst} > a$ and $\rho_{inst} << L$, with L the spatial extent of the lattice. These present no problems however, as the continuum instanton action,

$$S^{inst} = \frac{8\pi^2}{g^2}, \tag{3.16}$$

although scale-invariant classically, has a dependence on ρ_{inst} at first order [14, 15] at the quantum level, implying that for physical instantons,

$$\lim_{\rho \to 0} S_{inst}(\rho) \to \infty. \tag{3.17}$$

This has the effect that perturbative scale instantons have extremely high action, and so are unphysical. Thus, the UV regulator of the lattice spacing does not remove any important physics. Numerical studies [15] have shown that the physical size of instantons is $\mathcal{O}(0.3\,\mathrm{fm})$, while we use large lattices of size $2.52\,\mathrm{fm} \times 5.04\,\mathrm{fm}$.

Following [29], the Wilson gauge action(eq. 2.15) can be expanded in powers of a as

$$\begin{aligned} S_W \quad = \quad & \sum_{x,\mu,\nu} \mathrm{Tr}[-\frac{a^4}{2}F_{\mu\nu}^2 + \frac{a^6}{24}((\mathbf{D}_\mu F_{\mu\nu}(x))^2 + (\mathbf{D}_\nu F_{\mu\nu}(x))^2) \\ & -\frac{a^8}{24}\{F_{\mu\nu}^4(x) + \frac{1}{30}((\mathbf{D}_\mu^2 F_{\mu\nu}(x))^2 + (\mathbf{D}_\nu^2 F_{\mu\nu}(x))^2) \\ & +\frac{1}{3}\mathbf{D}_\mu^2 F_{\mu\nu}(x)\mathbf{D}_\nu^2 F_{\mu\nu}(x) - \frac{1}{4}(\mathbf{D}_\mu \mathbf{D}_\nu F_{\mu\nu}(x))^2\}] \end{aligned} \tag{3.18}$$

where $\mathbf{D}_\mu f = [D_\mu, f]$ for arbitrary f. We can then substitute $A_\mu(x)$ into this to acquire the local action around an instanton, giving [29]

$$S_w^{inst} = \frac{8\pi^2}{g^2}[1 - \frac{1}{5}(\frac{a}{\rho_{inst}})^2 - \frac{1}{70}(\frac{a}{\rho_{inst}})^4 + \mathcal{O}(a^6)]. \tag{3.19}$$

This immediately reveals the source of the problem; although at first order this is equivalent to the continuum action, the leading error term is strictly negative, and inversely dependent on ρ_{inst}. This implies that the only way to reduce the action around the neighbourhood of a instanton is by shrinking the instanton, and so smearing algorithms will make instantons smaller, particularly given repeated sweeps. This leaves us in the unfortunate position of not being able to isolate instanton effects without destroying the topological structure of the vacuum.

The heart of the problem is the approximation to the continuum gluonic action made by the Wilson action; discretisation errors reduce the size of the instanton, and so we hope that by using a different discretisation we can solve the issue.

The obvious first choice is the Symanzik action, eq. (2.24), expanded in powers of a as [29]

$$\begin{aligned} S_{Symanzik} &= \sum_{x,\mu,\nu} \mathrm{Tr}[-\frac{a^4}{2}F_{\mu\nu}^2(x) + \frac{a^8}{24}(F_{\mu\nu}^4(x) + \frac{1}{3}\mathbf{D}_\mu^2 F_{\mu\nu}(x)\mathbf{D}_\nu^2 F_{\mu\nu}(x) \\ &\quad -\frac{1}{4}(\mathbf{D}_\mu\mathbf{D}_\nu F_{\mu\nu}(x))^2 + \frac{4}{15}(\mathbf{D}_\mu^2 F_{\mu\nu})^2)] + \mathcal{O}(a^{10}). \end{aligned} \tag{3.20}$$

Again substituting the continuum infinite volume instanton solution, we arrive at

$$S_{Symanzik}^{inst} = \frac{8\pi^2}{g^2}[1 - \frac{17}{210}(\frac{a}{\rho_{inst}})^4 + \mathcal{O}(a^6)]. \tag{3.21}$$

This shows that merely removing the lower order error terms is insufficient to preserve instantons; the $\mathcal{O}(a^4)$ term is still negative, and so we expect success sweeps of smearing to remove instantons, although this process should be slower than using the Wilson action, as the negative term is higher order. The Symanzik improved action has been shown in lattice simulations to have no stable instantons [28], confirming this prediction. It is clear that in order

to make stable instantons exist on the lattice through smearing, we must make the first order error term positive. This idea was first implemented in [29], which modified the Wilson action to include a free parameter ϵ, which could be set negative in order to preserve instantons. This is known as over-improved smearing, and forms the basis of the work done here. Here however, we follow the work of [34] and use 1×1 and 2×1 rectangles rather than the 2×2 squares used in [29]. This reduces the number of links in each rectangle to 6, minimising the order of u_0 used, and hence reducing errors. The parameter ϵ is introduced by requiring that $\epsilon = 0$ gives the Symanzik action, and $\epsilon = 1$ gives the Wilson action. ϵ can be viewed as quantifying the degree to which the standard Wilson action is 'improved' by addition of rectangular loops, and so the choice of the name over-improved smearing for negative ϵ becomes clear. Explicitly, the new action is given by;

$$S_{over-improved}(\epsilon) = \frac{2}{g^2}\sum_x\sum_{\mu>\nu}[\frac{5-2\epsilon}{3}(1-P_{\mu\nu}) - \frac{1-\epsilon}{12}(1-R_{\mu\nu})]. \quad (3.22)$$

The usual expansion in powers of a gives

$$\begin{aligned} S_{over-improved}(\epsilon) &= a^4\sum_x\sum_{\mu>\nu}\mathrm{Tr}[\frac{1}{2}F^2_{\mu\nu}(x) - \frac{\epsilon a^2}{24}((\mathbf{D}_\mu F_{\mu\nu}(x))^2 + (\mathbf{D}_\nu F_{\mu\nu}(x))^2) \\ &+\frac{a^4}{24}(g^2(1-2\epsilon)F^4_{\mu\nu}(x) + \frac{5\epsilon-4}{30}((\mathbf{D}^2_\mu F_{\mu\nu}(x))^2 + (\mathbf{D}^2_\nu F_{\mu\nu}(x))^2) \\ &+\frac{2\epsilon-1}{3}\mathbf{D}^2_\mu F_{\mu\nu}(x) + \frac{1-2\epsilon}{4}(\mathbf{D}_\mu\mathbf{D}_\nu F_{\mu\nu}(x))^2)] + \mathcal{O}(a^{10}), \end{aligned} \quad (3.23)$$

then substituting the instanton solution,

$$S^{inst}_{over-improved}(\epsilon) = \frac{8\pi^2}{g^2}[1 - \frac{\epsilon}{5}(\frac{a}{\rho_{inst}})^2 + \frac{14\epsilon-17}{210}(\frac{a}{\rho_{inst}})^4]. \quad (3.24)$$

As by design, negative values of ϵ will lead to a positive first error term, and instantons are preserved under smearing. This introduces a new problem however; a positive first order error term will enlarge instantons proportionally to their radius, and so can distort their true shape. The new gauge action is introduced into stout-link smearing by redefining $C_\mu(x)$ to have the form

$$C_\mu(x) = \rho_{\mu\nu}\sum_\nu[\frac{5-2\epsilon}{3}(\Xi_{\mu\nu})(x) - \frac{1-\epsilon}{12}(L_{\mu\nu}(x))]. \quad (3.25)$$

where we have defined the 'long staples' $L_{\mu\nu}(x)$ analogously to the staples $\Xi_{\mu\nu}(x)$. $L_{\mu\nu}(x)$ are all 2×1 and 1×2 rectangles in the $\mu\nu$ plane including $U_\mu(x)$, with $U_\mu(x)$ then removed. From this it is trivially clear that the symmetry properties shown above for stout-link smearing remain for over-improved stout link smearing.

Having chosen a smearing method, the obvious next step is to fix the parameters, ϵ and $\rho_{\mu\nu}$. An unnecessarily negative value of ϵ will result in instantons expanding, just as a positive ϵ results in their shrinking, distorting the gauge field from an approximation to the physical configuration. Additionally, large instantons can be destroyed by the smoothing procedure, as large ρ_{inst} reduces the action at the instanton center. It was shown in [34] that a choice of $\epsilon = -0.25$ and constant $\rho = 0.06$ results in desirable behaviour, by showing that this choice leads to a ratio of $\frac{S_{over-improved}(\epsilon)}{S_{continuum}}$ that is closest to 1 for instantons of size $\frac{\rho_{inst}}{a} > 1$, and that the excess growing of instantons is restricted to 0.1% of their size per sweep at worst.

3.3 Measuring Instanton Properties on the Lattice

Our aim is to produce a set of configurations where instanton effects dominate the gauge field. This naturally raises a number of questions; will smearing produce this liquid state? How many sweeps will be needed to ensure it is dominated by instanton effects? How close to continuum instantons are they? At what point does the positive error term in the instanton action begin to unnecessarily enlarge the instantons?

This balance of smearing involves an unavoidable level of subjectivity; in order to minimise this we will measure the properties of topological objects on the lattice, and with reference to the predictions of the instanton liquid model choose a level of smearing which will create lattice topological objects resembling continuum instantons as closely as possible. Numerical simulations [15, 26] have shown that once revealed on the lattice, instantons closely adhere to most desirable properties, such as self-duality and localisation of their action density, so here we focus on the optimal number of sweeps of

smearing to create optimal instantons.

The work in [36] suggests that qualitatively, after 20 sweeps of smearing the topological objects discovered on the lattice closely approximate the instanton solution, and also examined the percentage of points within the radius of these objects which are charge coherent with the center, showing that within approximately half the radius, lattice points are almost all charge coherent.

This previous work gives confidence that smearing reveals a topological structure qualitatively similar to that of the instanton liquid model. We will extend this here, seeking to remove subjectivity as much as possible by defining a diverse varienty of quantitative measures of the effect of smearing on the topology of lattice gauge fields. Through this we hope to find an optimal level of smearing which will produce a smeared gauge field configuration closely resembling the long-range structure of the unsmeared configuration, taking care to smear enough to completely remove short-range effects while keeping the distortion of topological objects minimal.

We will examine 10 lattices with up to 300 sweeps of smearing, and locate points which are local maxima of the action; that is points which have a larger action than any in the surrounding hypercube. This is then taken as the approximate center of an instanton, around which we fit the classical instanton action density,

$$S_0(x) = \xi \frac{6}{\pi^2} \frac{\rho_{inst}^4}{((x - x_0)^2 + \rho_{inst}^2)^4} \tag{3.26}$$

where x_0 is the center of the instanton and ξ is a scale parameter. We have introduced the parameter ξ to allow the shape of the action around the point to determine the fit; we expect the lattice to have a higher action in general than the classical case, and so we wish the height to be irrelevant. We will then compare to the topological charge at the center for an (anti)instanton

$$q(x_0) = Q \frac{6}{\pi^2 \rho_{inst}^4} \tag{3.27}$$

where $Q = \mp 1$ for an (anti)instanton.

This gives us a list of instanton candidates with their position, shape and size. We expect that for low levels of smearing this will include a large

number of false positives, local maxima of the action density bearing little resemblance to an instanton. We will therefore perform a variety of analyses on this data to discern a level of smearing which removes these from the lattice, as well as to probe the structure of our topological objects.

First we provide a graph of extrapolated topological charge at the center vs ρ, hoping to observe the charge relation above. Figures (3.1a-3.1j) show up to 100 sweeps of smearing for a given single configuration, in intervals of 10 sweeps, with the theoretical topological charge lines also plotted.

We can immediately see results similar to [36]. The number of instanton candidates starts out large, and distributed fairly evenly around sizes of 2-8 lattice units, with little correlation to the predicted charge lines. This quickly changes as the number of sweeps increases, eventually leading to a very close fit. The number of instanton candidates also drops off rapidly at first, then steadily decreases. By the 50 sweeps mark we can be confident that almost all local maxima found closely approximate an instanton near the center. To attempt to quantify these observations, we will study the data from all 10 configurations and every level of sweeping. To make this subjective analysis more quantitative, we define the distance of each instanton candidate from the theoretical fit line as the distance from the theoretical relationship, DfTR,

$$\min[(\rho-\rho_0)^2+(\frac{6}{\pi^2\rho^4}-q_0)^2]. \tag{3.28}$$

To evaluate this, we find the zero of the derivative

$$\begin{aligned} 2(\rho-\rho_0)+2(\frac{6}{\pi^2\rho^4}-q_0)\frac{6}{\pi^2}\frac{-4}{\rho^5}&=0 \\ 2\rho-\rho_0+\frac{48q_0}{\pi^2\rho^5}-\frac{288}{\pi^4\rho^9}&=0. \end{aligned} \tag{3.29}$$

However the ρ^{-9} term creates highly singular behaviour near the 0, and we expect results to be $\mathcal{O}(10^{-3})$ or similar from inspection of the graph. Thus we multiply through by ρ^9 to find solutions of

$$f(\rho)=2\rho^{10}-\rho_0\rho^9+\frac{48q_0\rho^4}{\pi^2}-\frac{288}{\pi^4}=0. \tag{3.30}$$

This is done using Newton's Method,

$$\rho_{n+1}=\rho_n-\frac{f(\rho)}{f'(\rho)}, \tag{3.31}$$

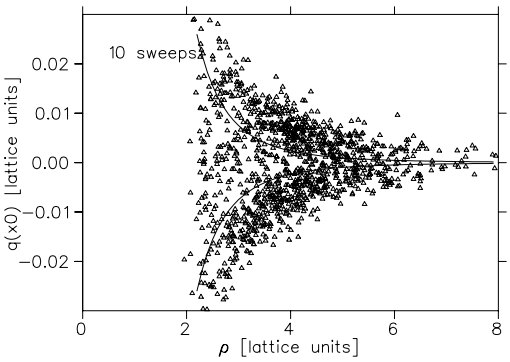

(a) 10 sweeps of smearing

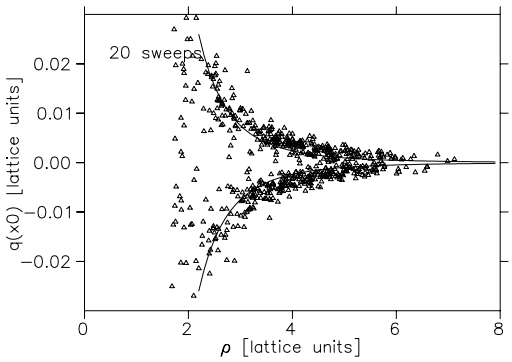

(b) 20 sweeps of smearing

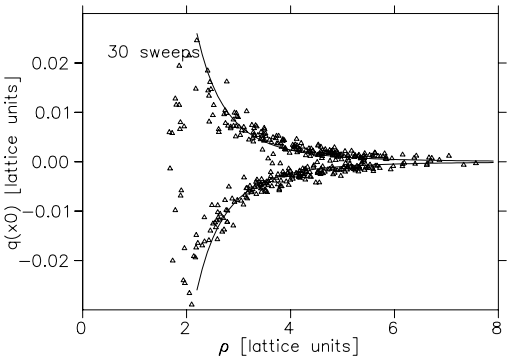

(c) 30 sweeps of smearing

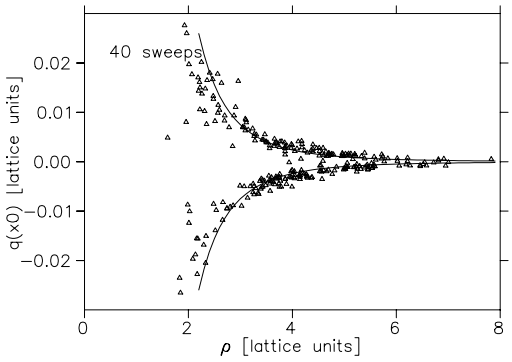

(d) 40 sweeps of smearing

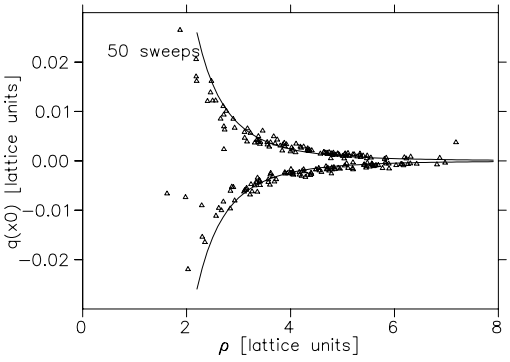

(e) 50 sweeps of smearing

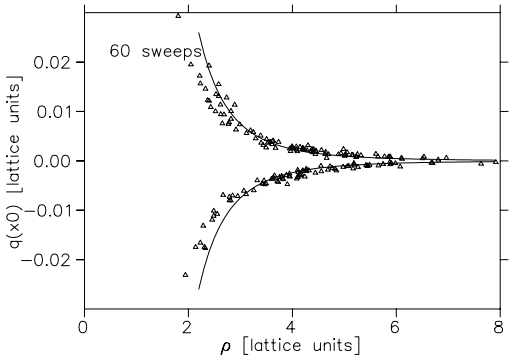

(f) 60 sweeps of smearing

Figure 3.1: The fitted values of instanton ρ plotted against q_{x0} at various levels of smearing

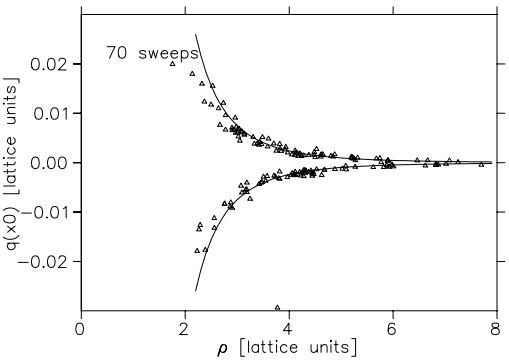

(g) 70 sweeps of smearing

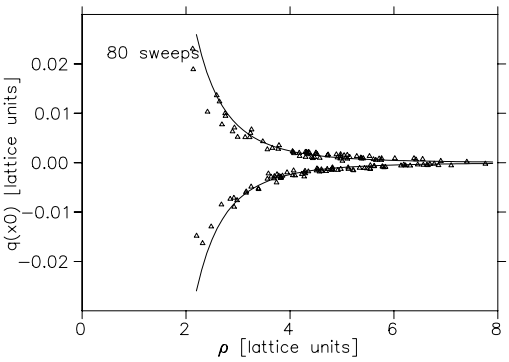

(h) 80 sweeps of smearing

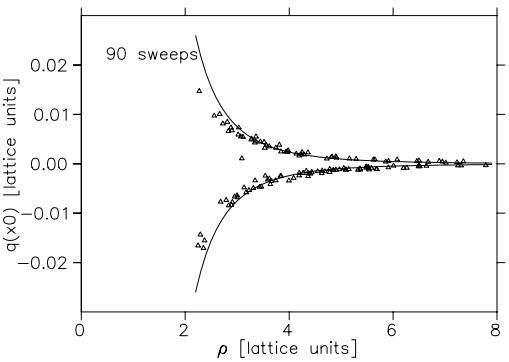

(i) 90 sweeps of smearing

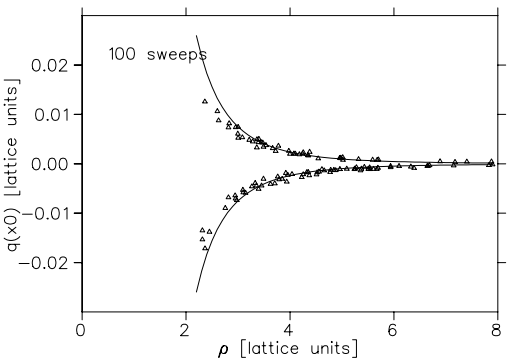

(j) 100 sweeps of smearing

Figure 3.1: The fitted values of instanton ρ plotted against q_{x0} at various levels of smearing

giving

$$\rho_{n+1} = \rho_n - \frac{2\rho^{10} - \rho_0\rho^9 + 48q_0\rho^4\pi^{-2} - 288\pi^{-4}}{20\rho^9 - 9\rho_0\rho^8 + 192q_0\rho^3\pi^{-2}}. \tag{3.32}$$

We iterate until errors are less than 10^{-9}. Figure (3.2) shows the DfTR,

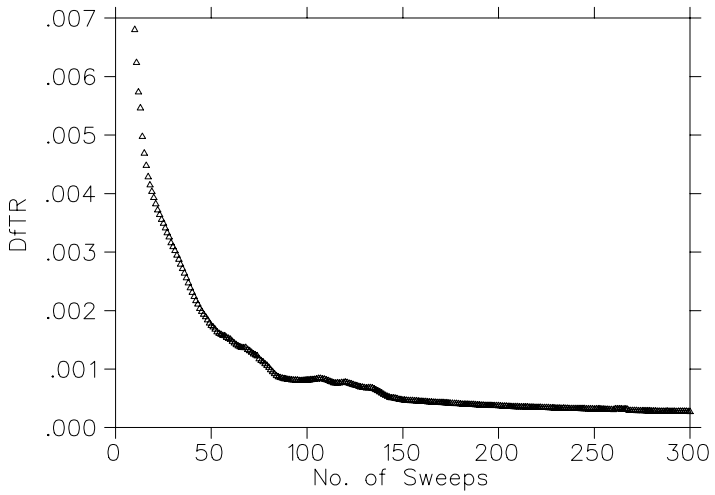

Figure 3.2: Distance from the theoretical relation between topological charge at the centre of instantons and their radius

confirming our earlier observations; before 50 sweeps, the DfTR decreases very rapidly as noise is removed from the lattice, before steadily decreasing afterward. This suggests there is little benefit in smearing beyond 100 sweeps, and the optimal level should lie somewhere in the 50-100 zone, most likely in the 70-80 range where the graph begins to plateau. Figure (3.3) shows the average density of instanton candidates. This shows that the density decreases rapidly until around 70 sweeps, then slowly, confirming our suspicion that by this time almost all fluctuations have been removed by the smearing algorithm, and only instanton-like objects remain. Figure (3.4) shows the average radius of instanton candidates. This shows that after a relatively steep initial decline, attributable to large short-scale fluctuations being destroyed quickly by the smearing algorithm, the average radius of instanton candidates steadily increases. This is an artifact of the positive error term in

the smearing; we cannot continue to use smearing freely without distorting the picture of the vacuum, beyond around 100 sweeps this enlarging effect becomes greater than 10%, and so we cannot rely on results in this region to accurately depict vacuum structure. To illustrate this, we plot a histogram of instanton radius, figure (3.5). We can clearly see that at high levels of smearing instantons are much larger, while we can perform up to 100 sweeps without drastically changing their size.

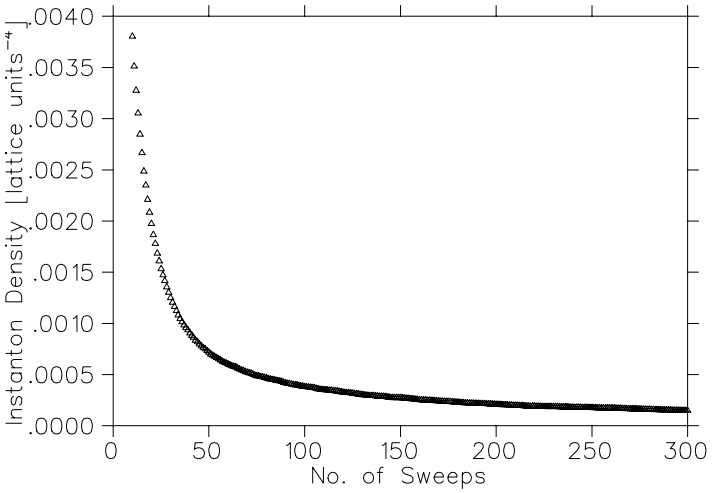

Figure 3.3: Average density of instanton candidates on the lattice

Up until now, we have analysed only the fit to eq. (3.26) based mainly on the center of the instanton candidate. We can measure the extent to which the vacuum structure within candidates approximates a classical instanton, by finding the percentage of lattice sites within a given distance which have the same sign of topological charge as at the center. Figure (3.6) shows this at 50% of each instanton's fitted radius. We see strong coherence for large values of smearing, suggesting our objects are very similar to continuum instantons in structure. For smearing below ≈ 50 sweeps, coherence is poor even this close to the center of the object. This reinforces that at these levels, we have fitted to a large number of false positives, indirectly showing that

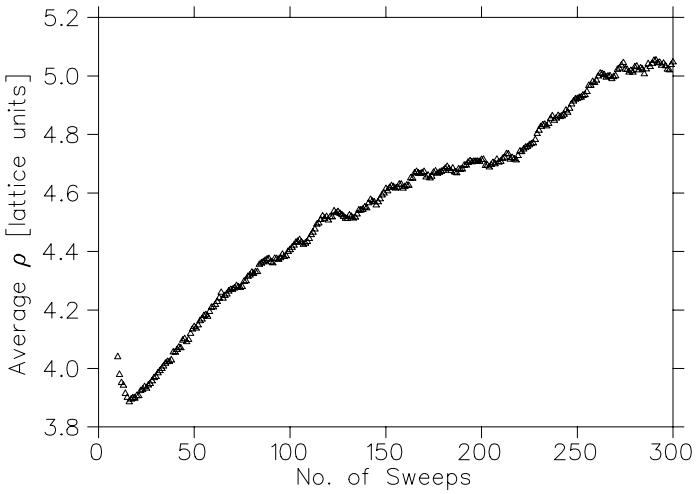

Figure 3.4: Average radius of instanton candidates

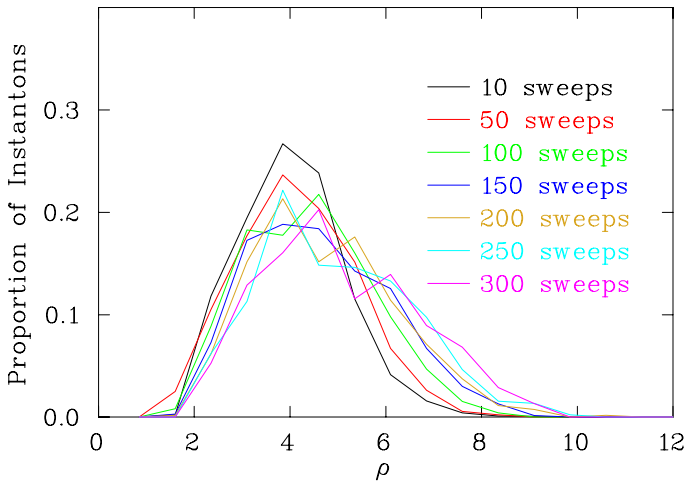

Figure 3.5: A histogram of ρ

the vacuum still has short-range effects here.

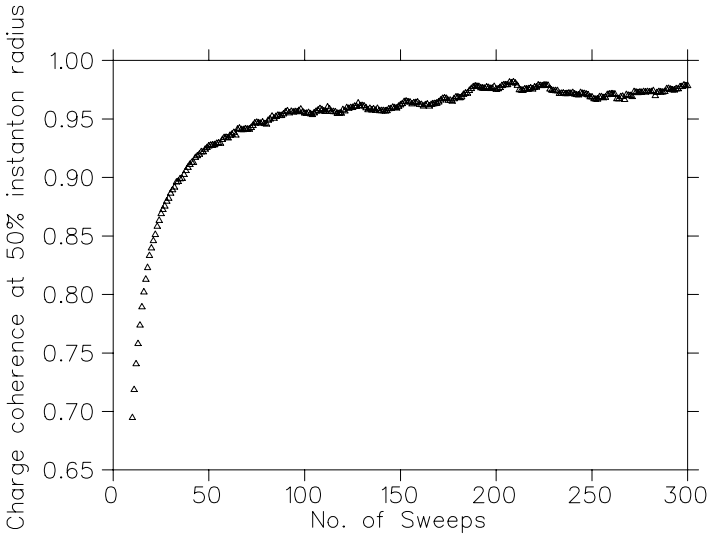

Figure 3.6: Topological Charge Coherence within 50% of the instanton radius

We can also examine how well our fitted ρ portrays the actual extent of the instantons found on the lattice by graphing the coherence at the instanton radius, Figure (3.7). Here we see that even at high levels of smearing, we reach only $\approx 85\%$ coherence, suggesting that the fitted ρ from the centre of the instanton overestimates the size of instantons.

Aggregating these measures, we define the Instanton Quality Index as

$$\mathrm{IQI} = \frac{\mathrm{DfTR}(\rho_{av} - \rho_0)^2(1 - C_{0.5\rho})}{N_{inst}} \tag{3.33}$$

where N_{inst} is the number of instanton candidates, ρ_0 the initial average instanton candidate radius and $C_{0.5\rho}$ the charge coherence at 50% of ρ. The minimal value of this should provide the optimal level of smearing, with the proviso that regardless of the other measures, a large deviation from ρ_0 gives unacceptable results. Thus we will restrict our consideration to the already identified important region of up to 120 sweeps.

Graphing this in (3.8), we see that the already identified important region of 80 sweeps provides an optimal value, beyond which the IQI plateaus. We

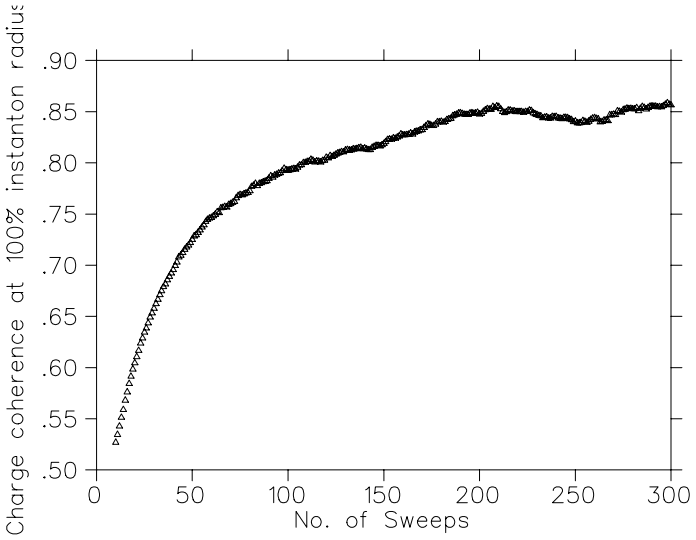

Figure 3.7: Topological Charge Coherence within the instanton radius

will thus perform calculations on up to 100 sweeps of smearing, with intervals 30, 50, 80 and 100.

Although we have created lattice configurations with a vacuum structure qualitatively very similar to the instanton liquid model, it is useful to compare quantitative details. We find an average radius of $\rho_{av} \approx 4a = 0.504\,\mathrm{fm}$, in contrast to the ILM prediction of $\frac{1}{3}\,\mathrm{fm}$, and an average density $\approx \frac{0.0005}{a^4} = 2\,\mathrm{fm}^{-4}$, compared to $1\,\mathrm{fm}^{-4}$. These both suggest a vacuum which is far 'fuller' than expected. In figure (3.9) we plot the packing fraction on our configurations. As we have previously seen that ρ is not an ideal measure of the extent of lattice topological objects, we use values calculated in two ways; that found by the fit to eq. (3.26) and using eq. (3.27). Although the two measures provide different values, it is clear that we have found a vacuum structure with far higher instanton content than that used in the ILM.

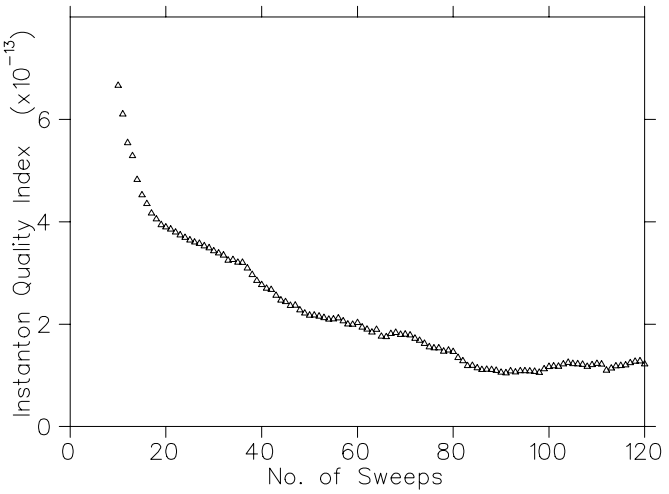

Figure 3.8: Instanton Quality Index as a function of number of sweeps.

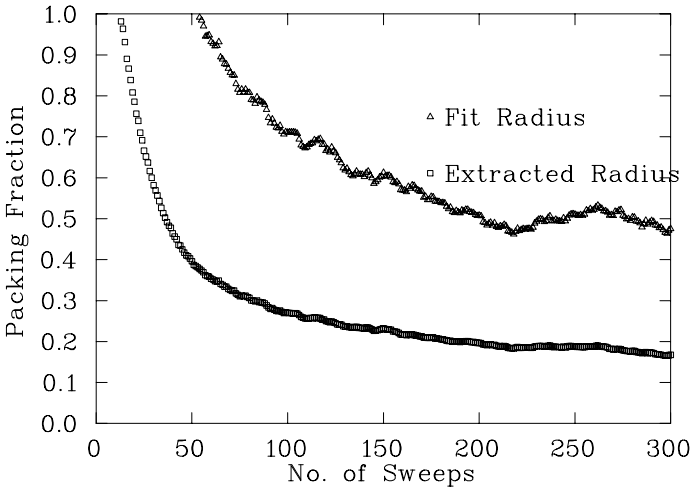

Figure 3.9: Packing Fraction of Instantons, the percentage of the vacuum composed of instantons

Chapter 4

The Overlap Propagator

4.1 The Fermion Doubling Problem and No-Go Theorem

Our chief topic of investigation is the quark propagator, and so it is vital that we choose a discretised fermion action carefully. It is not enough to merely ensure that we have the correct continuum limit; subtler aspects must be retained in order to produce meaningful results.

We begin by returning to the the naively discretised fermion action found in chapter 2, eq. (2.11),

$$\mathcal{S}^F_{free}(x) = \bar{\psi}(x)(\gamma^\mu \nabla_\mu + m)\psi(x), \tag{4.1}$$

suppressing the flavour sum and spatial dependence for brevity.

Closely examining this definition leads to an immediate problem; the central finite difference operator only couples lattice sites that are separated by $2a$. This leads to two uncoupled fermion fields in each dimension, and so $2^d = 16$ fermion fields altogether. This can also be seen by transforming the Dirac operator to momentum space, [38]

$$\begin{aligned}
\tilde{D} &= m + \int d^4x \gamma_\mu e^{-ip.x} \nabla_\mu \\
&= m + \int d^4x \gamma_\mu e^{-ip.x} \frac{1}{2a}(T_\mu(x) - T^\dagger_\mu(x)) \\
&= m + \frac{1}{2a} \int d^4x \gamma_\mu [e^{-ip.(x-a\hat{\mu})} - e^{-ip.(x+a\hat{\mu})}]
\end{aligned}$$

$$\begin{aligned} &= m + \frac{1}{2a}\gamma_\mu [\int d^4x [e^{iap.\hat{\mu}} - e^{-iap.\hat{\mu}}] e^{-ip.x} \\ &= m + \frac{1}{2a}\gamma_\mu [e^{iap_\mu} - e^{-iap_\mu}] \\ &= m + \frac{i}{a}\gamma_\mu \sin(ap_\mu), \end{aligned}$$

giving as the inverse of the free field propagator,

$$S^{-1}(p) = m + \frac{i}{a}\gamma^\mu \sin(ap_\mu) \tag{4.2}$$

noting that here S refers to the propagator, not the action. The source of the problem is now clear; in the limit $m \to 0$, the propagator has 16 zeroes in the Brillouin zone, at $p = (0,0,0,0), p = (\frac{\pi}{a},0,0,0), p = (\frac{\pi}{a},\frac{\pi}{a},0,0)$ etc. This leads to the 16 fermion species, and so we must try to find an action that couples all sites, and thus fourier transforms to an inverse propagator with only one zero.

The first proposed solution was introduced by Wilson [39], who added an additional term corresponding to a discretised 'Laplacian' operator. Given the definition

$$\triangle_\mu \psi(x) = \frac{1}{a^2}[2 - T_\mu(x) - T_\mu^\dagger(x)]\psi(x), \tag{4.3}$$

the Wilson fermion action is given by [40],

$$S_W = \bar{\psi}(\not{\nabla} + \frac{ra}{2}\sum_\mu \triangle_\mu + m)\psi \tag{4.4}$$

where r is the Wilson Coefficient, canonically set to 1. Definition 4.3 shows why this removes the problem; this term now couples all sites. We can also fourier transform the additional term to see this in momentum space,

$$\begin{aligned} \mathcal{F}\Big(\bar{\psi}\triangle_\mu\psi\Big) &= \frac{2}{a^2}\tilde{\bar{\psi}}\tilde{\psi} - \frac{1}{a^2}\tilde{\bar{\psi}}\int d^4x e^{-ip.x}\triangle_\mu\psi \\ &= \frac{2}{a^2}\tilde{\bar{\psi}}\tilde{\psi} - \frac{1}{a^2}\tilde{\bar{\psi}}\int d^4x [e^{-ip.x}\psi(x+a\hat{\mu}) + \psi(x-a\hat{\mu})] \\ &= \frac{2}{a^2}\tilde{\bar{\psi}}\tilde{\psi} - \frac{2}{a^2}\tilde{\bar{\psi}}\cos(ap_\mu)\tilde{\psi}. \end{aligned}$$

The cosine term only has a zero at $p_\mu = 0$, and so the the doubled species are removed. Effectively, we have given all extra species a mass proportional to $\frac{1}{a}$; as we take the continuum limit $a \to 0$, their mass tends to infinity.

This solution of the doubling problem comes with an issue however, when we consider chiral symmetry. A famous result in continuum QCD is chiral invariance in the massless case; that is, invariance under the transformation

$$\psi(x) \to e^{i\alpha\gamma_5}\psi(x) \qquad \bar{\psi}(x) \to \bar{\psi}(x)e^{i\alpha\gamma_5}. \tag{4.5}$$

This can easily be shown for the naively discretised lattice fermion action in the case $m = 0$ [38]. Noting first that at $\mathcal{O}(\alpha)$, a chiral transformation is given by

$$\psi(x) \to (1 + i\alpha\gamma_5)\psi \qquad \bar{\psi(x)} \to \bar{\psi}(1 + i\alpha\gamma_5), \tag{4.6}$$

we find

$$\begin{aligned} S' &= \bar{\psi}(1 + i\alpha\gamma_5)\gamma^\mu\nabla_\mu(1 + i\alpha\gamma_5)\psi \\ &= \bar{\psi}\gamma^\mu\nabla_\mu\psi + \bar{\psi}(i\alpha\gamma_5\gamma^\mu\nabla_\mu + \gamma^\mu\nabla_\mu i\alpha\gamma_5)\psi + \prime(a^2) \\ &= \bar{\psi}\gamma^\mu\nabla_\mu\psi + i\alpha\bar{\psi}\{\gamma_\mu, \gamma_5\}\nabla_\mu\psi \\ &= \bar{\psi}\gamma^\mu\nabla_\mu\psi \\ &= S. \end{aligned} \tag{4.7}$$

From this it is clear that anti-commutation with γ_5 is critical. An issue with the Wilson action is now obvious; it does not anti-commute with γ_5 and so is not chirally symmetric. This has several important consequences, but the most important here is that without any protection from chiral symmetry, the massless case is no longer distinguished and so the quark mass suffers from additive mass renormalisation. This has several undesirable effects; it allows eigenvalues of the Dirac operator near 0, greatly damaging the key determinant of inversion speed, the condition number, $\frac{\lambda_{\max}}{\lambda_{\min}}$. More worryingly here, however, it significantly complicates the relationship between the lattice quark propagator and the mass function. The simplest way to fix this seems clear; create a fermion action which is chirally symmetric while still removing the doublers. Unfortunately, this conflicts with a famous lattice theorem, the Nielsen-Ninomiya No-Go Theorem [41, 42, 43], which explicitly states [44] given;

- A quadratic fermion action $\bar{\psi}(x)iH(x-y)\psi(y)$, where H is Hermitian, has a Fourier transform $H(p)$ defined for all p in the Brillouin zone,

and has a continuous first derivative everywhere in the Brillouin zone. $H(p)$ should behave as $\gamma_\mu p_\mu$ for small p_μ.

- A local conserved charge Q defined as $Q = \sum_x j_0(x)$, where j_0 is a function of the field variables $\psi(y)$ where y is close to x.
- Q is quantised

Then $H(p)$ has an equal number of left- and right-handed fermions for each eigenvalue of Q. Roughly speaking, this means it is impossible to have a fermion action that is chirally symmetric, free of doublers and local. Of these, chiral symmetry is the only one that can reasonably be sacrificed, and so most lattice fermion actions explicitly break chiral symmetry, with unfortunate implications for mass renormalisation.

The no-go theorem, however, only prohibits an explicitly chirally symmetric action. Shortly after the theorem was derived, Ginsparg and Wilson [45] showed that if continuum chiral symmetry were 'minimally' broken, by the relation

$$\gamma_5 D + D\gamma_5 = 2aD\gamma_5 D, \tag{4.8}$$

then the propagator would anti-commute with γ_5 at non-zero distances, and so a remnant of chiral symmetry would be present. This can be shown [46] to be equivalent to a new exact symmetry of the form

$$\delta\psi = \gamma_5(1 - \frac{1}{2}aD)\psi \qquad \delta\bar{\psi} = \bar{\psi}(1 - \frac{1}{2}aD)\gamma_5. \tag{4.9}$$

This lattice version of chiral symmetry is enough to prevent additive mass renormalisation [47], while avoiding conflict with the no-go theorem.

4.2 Improved Fermion Actions

Before attempting to define a fermion action satisfying the Ginsparg-Wilson relation, it is useful to further improve the Wilson action. Analogously to our improvement of the gluon action in section 2.3, we can do this by choosing higher order terms to cancel first order errors. Following the derivation in [5], we write the QCD action in the form

$$S_{QCD} = \int \mathrm{d}^4x \Big[\mathcal{L}^{(0)} + a\mathcal{L}^{(1)} + a^2\mathcal{L}^{(2)} + ...\Big] \tag{4.10}$$

where $\mathcal{L}^{(i)}$ are terms of dimension $i+4$. Thus $L^{(0)}$ must be the usual QCD Lagrangian, and we are interested in setting $L^{(1)} = 0$. Using symmetry arguments, it can be shown that the only possible terms composing $L^{(1)}$ are linear combinations of

$$\begin{aligned}
\mathcal{L}_1^{(1)} &= \bar{\psi}\sigma_{\mu\nu}F_{\mu\nu}\psi \\
\mathcal{L}_2^{(1)} &= \bar{\psi}D_\mu^2\psi + [D_\mu^2\bar{\psi}]\psi \\
\mathcal{L}_3^{(1)} &= m\mathrm{Tr}[F_{\mu\nu}F_{\mu\nu}] \\
\mathcal{L}_4^{(1)} &= m\Big(\bar{\psi}\gamma_\mu D_\mu\psi - [D_\mu\bar{\psi}\gamma_\mu]\psi\Big) \\
\mathcal{L}_5^{(1)} &= m^2\bar{\psi}\psi
\end{aligned} \tag{4.11}$$

with the definition

$$\sigma_{\mu\nu} = \frac{[\gamma_\mu, \gamma_\nu]}{2i}. \tag{4.12}$$

We can reduce the number of possible operators further using the Dirac equation, leading to the relations

$$\begin{aligned}
\mathcal{L}_1^{(1)} - \mathcal{L}_2^{(1)} + 2\mathcal{L}_5^{(1)} &= 0 \\
\mathcal{L}_4^{(1)} + 2\mathcal{L}_5^{(1)} &= 0,
\end{aligned} \tag{4.13}$$

implying that we can absorb $\mathcal{L}_2^{(1)}$ and $\mathcal{L}_4^{(1)}$ into constant factors. $\mathcal{L}_3^{(1)}$ and $\mathcal{L}_5^{(1)}$ are present in $\mathcal{L}^{(0)}$ up to constant factors, and so we can redefine m and g to absorb these. Thus we can write an action, the Sheikholeslami-Wohlert [66] action, without $\mathcal{O}(a)$ errors by removing $\mathcal{L}_1^{(1)}$ terms from the Wilson action,

$$S_{sw} = S_{Wilson} + c_{sw}a^5\sum_{\mu<\nu}\bar{\psi}\frac{1}{2}\sigma_{\mu\nu}F_{\mu\nu}^{imp}\psi. \tag{4.14}$$

The coefficient c_{sw} can be mean field estimated as $c_{sw} = \frac{1}{u_0^3}$.

When simulating small quark masses, however, we encounter problems with even this highly improved action. To find the origin of this issue, we consider the eigenvalues of the massless Dirac operator, λ_i. Eigenvalues of the massive Dirac operator are given by

$$m + \lambda_i; \tag{4.15}$$

the λ_i are strongly dependent on the gauge field, and so the large short-distance fluctuations seen in gauge configurations can change their value greatly. If we have a configuration where $\lambda_k \approx -m$ for some k, known as an exceptional configuration, the Dirac operator will become singular and inversion next to impossible. To prevent this occurring, we can smear the gauge field as in chapter 3, which will also allow us to use the improved $F_{\mu\nu}$ operator with impunity. As we have seen, excess smearing can have deleterious effects on the topological structure of the gauge field, and so we perform smearing only on the physically irrelevant terms, ie those that are of dimension > 4. Thus we find the fat link irrelevant clover(FLIC) action, [67]

$$S_{flic} = \bar{\psi}(\not{\nabla} + \frac{a}{2}\sum_{\mu} \triangle_{\mu}^{fl} - \frac{1}{4}\sigma \cdot F^{\text{impfl}} + m)\psi \tag{4.16}$$

with irrelevant terms using 4 sweeps of stout-link smearing, as defined in 3.1.

4.3 The Overlap Action

An appropriate Dirac matrix satisfying the Ginsparg-Wilson relation, though initially elusive, was found with the definition of the overlap Dirac operator [48]. We present here a simplified derivation from ref. [49]. The central idea is to prepare for the momentum cutoff imposed by discretisation by compactifying the continuum Dirac operator, D_c. First note that the finite lattice spacing introduces a natural cutoff, $\Lambda = \frac{1}{a}$, which we should use as the limits of our compactification. We define an operator V_c using a Cayley transform on D_c,

$$V_c = \frac{D_c - \Lambda_c}{D_c + \Lambda_c}. \tag{4.17}$$

Then we can define a continuum D with compact spectrum via

$$D = \frac{1 + V_c}{1 - V_c}. \tag{4.18}$$

V_c, and thus D, inherit the important properties of γ_5 hermiticity and unitarity from D_c and are thus chirally symmetric. This is not sufficient in itself however; the lattice version must still obey the No-Go theorem, and so D

must be non-local. This problem can be solved though, by noting that terms $\mathcal{O}(\Lambda^2)$ are below the cutoff and thus irrelevant. Then we can expand V_c as

$$V_c = -1 + 2\frac{D_c}{\Lambda_c} + \text{irrelevant terms}, \tag{4.19}$$

and so

$$\frac{D_c}{\Lambda_c} = \frac{1+V_c}{2}. \tag{4.20}$$

This D_c has lost exact chiral symmetry, and so there is no longer a problem with the No-Go theorem. This means it should be possible to find some lattice V such that we can define a lattice D_0 by

$$D_0 = \frac{1+V}{2}. \tag{4.21}$$

The loss of exact chiral symmetry need not be debilitating; for our purposes it is sufficient to have a massive Dirac operator $D+m$ that is bounded away from 0 for $m \neq 0$. This will prevent the exceptional configuration problem seen earlier, as well as removing additive mass renormalisation. Consider

$$\begin{aligned}
(D+\frac{m}{\Lambda_c})^\dagger(D+\frac{m}{\Lambda_c}) &= (\frac{1+V_c}{2}+\frac{m}{\Lambda_c})^\dagger(\frac{1+V_c}{2}+\frac{m}{\Lambda_c}) \\
&= (\frac{m}{\Lambda_c}+\frac{1}{2}+\frac{V_c^\dagger}{2})(\frac{m}{\Lambda_c}+\frac{1}{2}+\frac{V_c}{2}) \\
&= \frac{m^2}{\Lambda_c}+\frac{m}{\Lambda_c}+\frac{V_c}{2}(\frac{m}{\Lambda_c}+\frac{1}{2})+\frac{V_c^\dagger}{2}(\frac{m}{\Lambda_c}+\frac{1}{2})+\frac{V_cV_c^\dagger}{4}.
\end{aligned}$$

Note that $D_c^\dagger = -D_c$ and V_c inherits this property through the Cayley transform, giving

$$\begin{aligned}
(\frac{1+V_c}{2}+\frac{m}{\Lambda_c})^\dagger(\frac{1+V_c}{2}+\frac{m}{\Lambda_c}) &= \frac{m^2}{\Lambda_c}+\frac{m}{\Lambda}+\frac{V_cV_c^\dagger}{4} \\
&\geq \min[\frac{m^2}{\Lambda}, (\frac{m}{\Lambda}+1)^2].
\end{aligned} \tag{4.22}$$

This testifies to the prospective success of the approach; we have a Dirac operator which can satisfy the No-Go theorem whilst being bound away from 0 for $\frac{m}{\Lambda} \neq 0, -1$. This prevents additive mass renormalisation, our desired property of chiral symmetry. This simplifies the problem to a search for an

appropriate lattice version of V. Noting that in the continuum, $G = \gamma_5 V_c$ obeys $G^2 = 1$ and $G^\dagger = G$, it seems natural to choose

$$G = \epsilon(\gamma_5 D) \tag{4.23}$$

where ϵ is the matrix sign function, $\epsilon(A) = \frac{A}{\sqrt{A^2}}$ and D is any reasonable Hermitian Dirac operator. Analysis [38] shows that in order to avoid doublers, we require $-2 < m < 0$. The exact value of m within this range is irrelevant. We also define the parameter κ_o by

$$\kappa_o = \frac{1}{[2ma + \frac{1}{\kappa_c}]} \tag{4.24}$$

where $\kappa_c = \frac{1}{8}$.

Thus we have the massless Overlap operator,

$$D_o = \frac{1}{2}(1 + \gamma_5 \epsilon(\gamma_5 D)). \tag{4.25}$$

The D chosen is referred to as the overlap kernel. The choice of kernel has significant effects on computation of the overlap, although it is irrelevant to the results, and will be discussed with more care later.

Verifying that this is a solution of the Ginsparg-Wilson relation is a simple task;

$$\begin{aligned} 2D_o\gamma_5 D_o &= \frac{1}{2}(1 + \gamma_5\epsilon(\gamma_5 H))\gamma_5(1 + \gamma_5\epsilon(\gamma_5 H)) \\ &= \frac{1}{2}[\gamma_5 + \gamma_5^2\epsilon(\gamma_5 H) + \gamma_5\epsilon(\gamma_5 H)\gamma_5 + \gamma_5\epsilon^2(\gamma_5 H)], \end{aligned}$$

remembering that $\gamma_5^2 = \epsilon^2 = I$,

$$\begin{aligned} &= \frac{1}{2}(\gamma_5 + \epsilon(\gamma_5 H) + \gamma_5\epsilon(\gamma_5 H)\gamma_5 + \gamma_5) \\ &= \gamma_5 D_o + D_o\gamma_5 \end{aligned} \tag{4.26}$$

as required.

Taking as overlap kernel the Wilson Dirac operator, 4.4, we can verify explicitly that the overlap has the correct continuum limit [38].

First we note

$$\begin{aligned} D_w^\dagger D_w &= (-\not{\nabla} + \frac{a}{2}\sum_\mu \triangle_\mu + m)(\not{\nabla} + \frac{a}{2}\sum_\mu \triangle_\mu + m) \\ &= m^2(1 - \frac{1}{m}(\not{\nabla} - \frac{a}{2}\sum_\mu \triangle_\mu))(1 + \frac{1}{m}(\not{\nabla} - \frac{a}{2}\sum_\mu \triangle_\mu)), \end{aligned} \tag{4.27}$$

then note that m has dimension $\frac{1}{a}$, implying ma is dimensionless, and so

$$D_w^\dagger D_w = m^2(1 + \mathcal{O}(a^2)). \tag{4.28}$$

Thus we have

$$\begin{aligned} D_o &= \frac{1}{2a}(1 + \gamma_5 \epsilon(\gamma_5 D)) \\ &= \frac{1}{2a}(1 + \gamma_5 \frac{\gamma_5 D}{\sqrt{D_w^\dagger D_w}}) \\ &= \frac{1}{2a}(1 + \gamma_5 \frac{\gamma_5 D}{\sqrt{m^2(1 + \mathcal{O}(a^2))}}) \\ &= \frac{1}{2a}(1 - \frac{1 - \frac{1}{m}(\not{\nabla} + \frac{a}{2}\sum_\mu \triangle_\mu)}{\sqrt{(1 + \mathcal{O}(a^2))}} \\ &= \frac{1}{2a}(1 - 1 + \frac{1}{m}(\not{\nabla} + \frac{a}{2}\sum_\mu \triangle_\mu)(1 - \mathcal{O}(a^2) \\ &= \frac{1}{2am}\not{\nabla} + \mathcal{O}(a) \\ &\to \frac{1}{2am}\not{D} \qquad \text{as } a \to 0. \end{aligned} \tag{4.29}$$

Finally, we relate the massless overlap operator,$D(0)$, to the massive,$D(\mu)$ by [38]

$$D(\mu) = (1 - \mu)D(0) + \mu, \tag{4.30}$$

representing a mass of $\frac{\mu}{1-\mu}$.

This presentation has left a small gap; although the overlap action itself only has 0 eigenmodes at $\mu = 0$, the overlap kernel explicitly breaks chiral symmetry, and so may have 0 eigenmodes for non-zero m. This is not a huge problem; only exactly 0 eigenvalues of the kernel will create a 0 eigenvalue

of the overlap, and the set of configurations containing these is of measure 0, and so does not appear in practice. These sign changing eigenvalues are not uninteresting however; they correspond to the presence of instantons, with a larger instanton causing a crossing at larger m, and the sign of the crossing denoting an instanton/anti-instanton [56, 57]. This leads to an alternate definition of the overlap topological charge,

$$Q = n_+ - n_- \tag{4.31}$$

where $n_\pm$ denotes the number of crossings of the relevant sign. This naturally partitions the set of all configurations, as a configuration cannot be smoothly deformed into one with a different value of Q without passing through a point where the action is undefined, restoring the continuum division of vacua. This topological charge should agree with that defined through the gauge field on highly smoothed configurations.

4.4 Calculating the Overlap Action

While this action may seem like it has cured our problems by making light quark masses viable, it has simultaneously introduced a new one; the evaluation of the matrix sign function. As we are required to evaluate the square root of the overlap kernel H, standard techniques for calculating the action fail. This is further compounded by the size of H, which on our lattices of dimensions $20^3 \times 40$ has $\mathcal{O}(10^{13})$ elements. This rules out direct storage of H, and thus usual solutions of the matrix square root. H is sparse however, so a solution remains possible. The standard approach, first developed by Neuberger [51, 52] is to approximate $\epsilon(H)$ as a sum of poles. Here we use the Zolotarev, or optimal rational polynomial approximation, given by [53, 38]

$$\epsilon(x) \approx \epsilon^n(x) = d_0 x(x^2 + c_{2n}) \sum_{l=1}^{n} \frac{b_l}{x^2 + c_{2l-1}}. \tag{4.32}$$

As we only change the constants in the sum, it can be evaluated using a single conjugate-gradient solution plus shifts [54]. The coefficients are functions of the condition number and the order of the approximation, and so are known ahead of time, given in [63].

The convergence speed of the conjugate-gradient algorithm is proportional to the condition number of H, κ. The spectrum of the usual choice of kernel, the Wilson-Dirac operator, is characterised by a small number of very low-lying eigenvalues and a dense region which lies higher. Thus it is clear how we can dramatically improve the condition number; by separating the low-lying eigenvectors and calculating them explicitly, we both reduce the range of eigenvalues, and move them farther from 0. It is here that choice of overlap kernel becomes important. Studies [58, 59, 60, 61] have shown that using a FLIC kernel greatly improves the low-lying spectrum, by both reducing the number of low eigenvalues and moving the dense region higher, resulting in a speedup of $\mathcal{O}(2)$. The next step is to produce plots of the low-lying spectrum of the FLIC operator on our lattices, to ascertain the number of eigenvectors we must deal with explicitly. Based on our results from smearing, we expect the low-lying spectrum to clear up rapidly with smearing sweeps, and so we calculate for 0, 10, 20 and 30 sweeps of smearing.

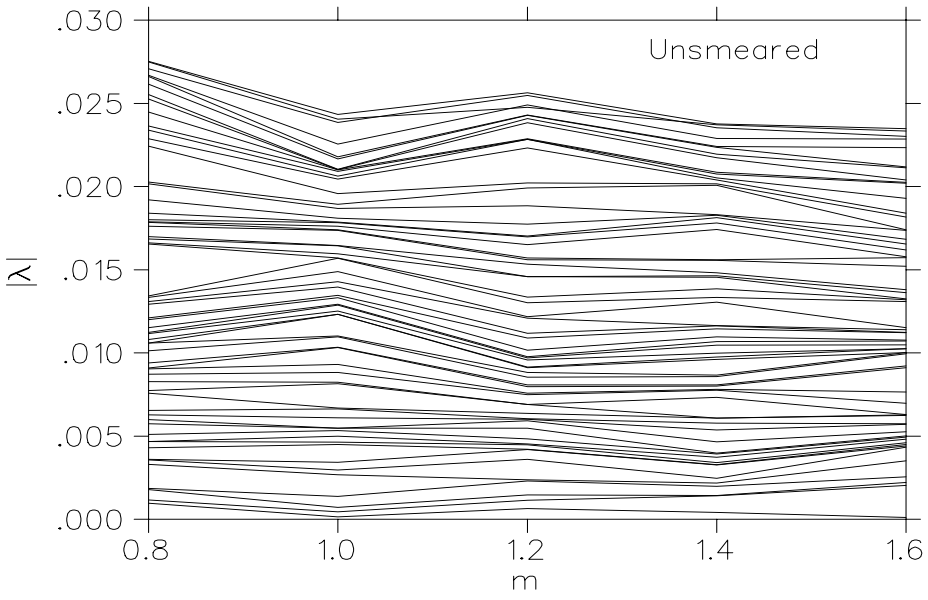

Figure 4.1: Spectral flow of the FLIC action on an unsmeared configuration

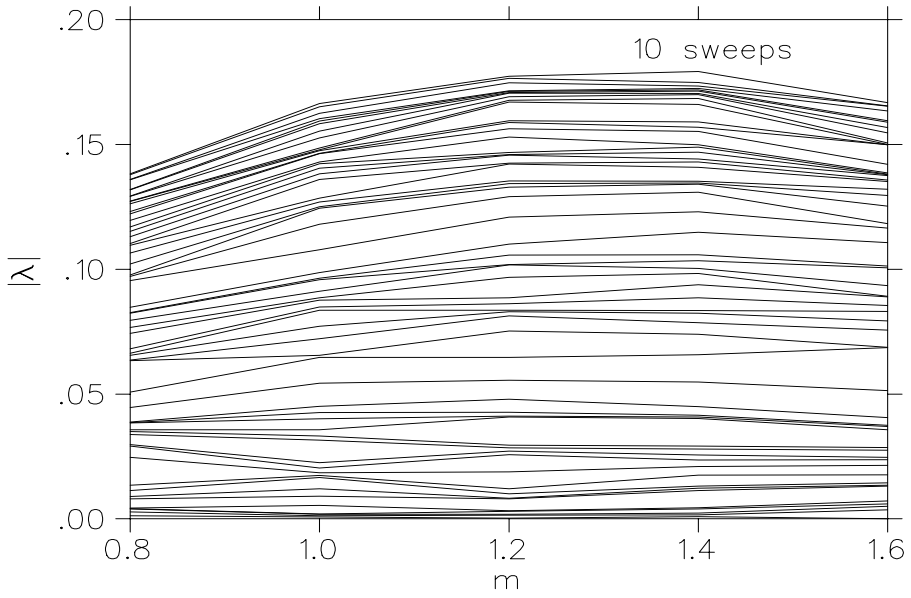

Figure 4.2: Spectral flow with 10 sweeps of smearing

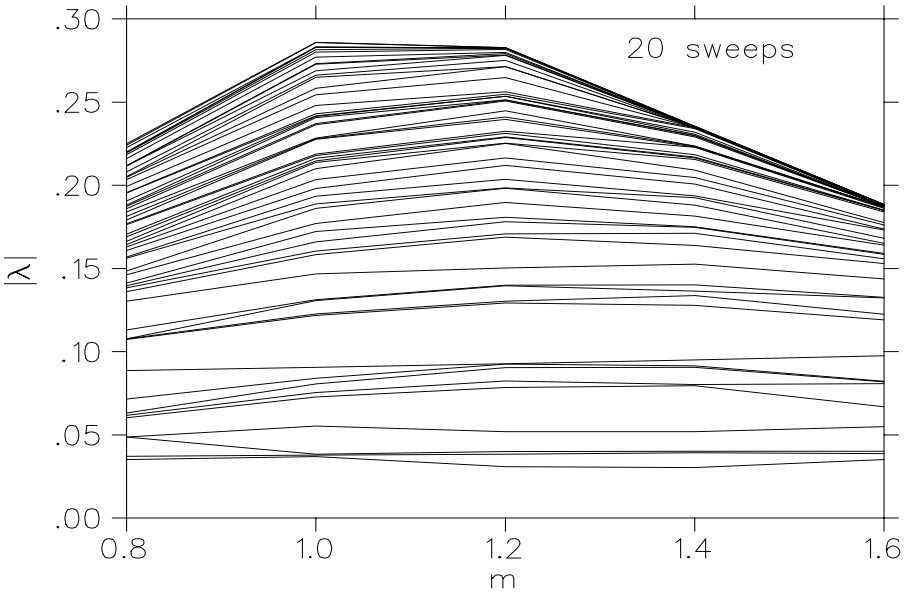

Figure 4.3: Spectral flow with 20 sweeps of smearing

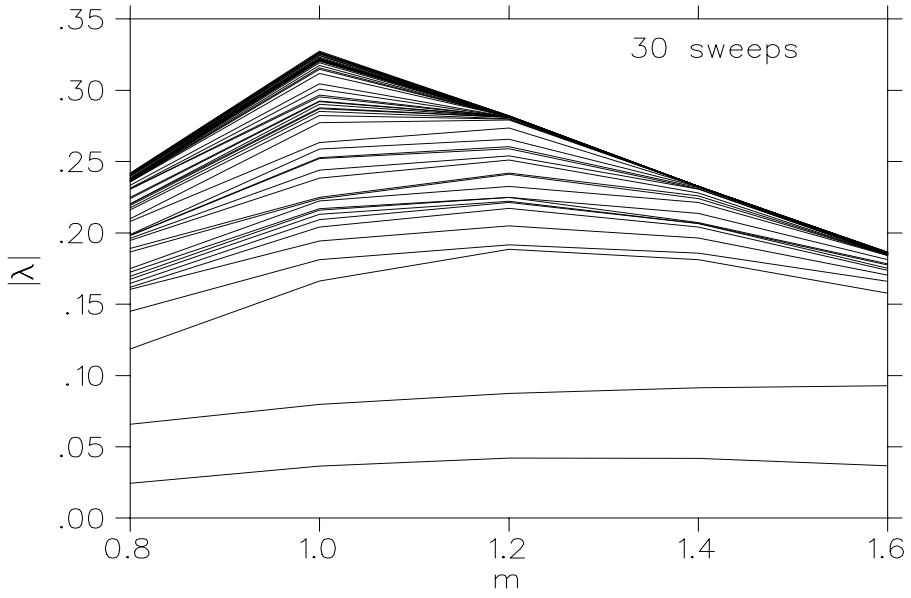

Figure 4.4: Spectral flow with 30 sweeps of smearing

Eigenvales were calculated at four points, evenly spaced between $m = 0.8$ and $m = 1.6$. Because of this relatively coarse resolution, it is difficult to see the presence of exact zeroes in these graphs.

As expected, the low-lying spectrum rapidly becomes cleaner with smearing. The unsmeared configurations need up to 55 low-lying eigenvectors extracted, but after 30 sweeps of smearing as few as 2 are required. We choose to extract 5 low-lying eigenvectors for configurations with 30 sweeps of smearing and upwards, as this more than covers the case shown here. For unsmeared configurations, we extract 55. From these graphs we also choose our value of m to use in calculations as $m = 1$, as this is the point where the eigenvalues for 30 sweeps peak, and the condition number is most favourable. We choose to use 13 values of μ, provided in table 4.4.

μ	m_{bare}(GeV)
0.01271	0.03980
0.01694	0.05305
0.02119	0.06637
0.02543	0.07965
0.02966	0.09290
0.03390	0.10618
0.04238	0.13274
0.05076	0.15898
0.06356	0.19908
0.08475	0.26545
0.10594	0.33182
0.12713	0.39819
0.14832	0.46456

Table 4.1: The 13 values of μ used, with the corresponding bare mass in physical units

Chapter 5

The Non-Perturbative Mass Function

5.1 Deriving the Mass Function

Having produced propagators, we now turn to creating the non-perturbative mass function. By comparing configurations with different levels of smearing, this will give us insight into dynamical mass generation. It is here that the use of the overlap shines; without additive mass renormalization it is possible to extract the mass and multiplicative renormalization with minimal tree-level correction. First recall that the overlap has correct continuum limit, eq. (4.29), [62]

$$\lim_{a\to 0} D_o = \frac{1}{2m_w} \not{p} \,. \tag{5.1}$$

It is then natural to define the massless bare overlap propagator in momentum space as [48]

$$S(p)_{massless} = \frac{1}{2m_w}(D_o^{-1} - 1), \tag{5.2}$$

as this ensures that we have

$$\{S(p)_{massless}, \gamma_5\} = 0. \tag{5.3}$$

Recalling the definition of the massive overlap operator, eq. (4.30), the massive overlap propagator is given by

$$S(p) = \frac{1}{2m_w(1-\mu)}(D_o^{-1} - 1). \tag{5.4}$$

We can define $\mathcal{C}$ and $\mathcal{B}$ by [64]

$$S^{bare}(p) = -i\not{\mathcal{C}}(p) + \mathcal{B}(p). \tag{5.5}$$

Noting that $\mathcal{B}(p)$ has no explicit colour or spin dependence.
Rearranging for $\mathcal{B}$,

$$\mathrm{Tr}(S^{bare}(p)) = \mathrm{Tr}(-i\not{\mathcal{C}}(p) + \mathcal{B}(p)), \tag{5.6}$$

using $\mathrm{Tr}(\gamma_\mu) = 0$,

$$\begin{aligned} \mathrm{Tr}(S^{bare}(p)) &= n_s n_c \mathcal{B}(p) \\ \mathcal{B}(p) &= \frac{1}{n_s n_c}\mathrm{Tr}(S^{bare}(p)). \end{aligned} \tag{5.7}$$

Similarly, we multiply by γ_ν and use $\mathrm{Tr}(\gamma_\mu\gamma_\nu) = 4$ to acquire

$$\mathcal{C}_\mu(p) = \frac{i}{n_s n_c}\mathrm{Tr}[\gamma_\mu S^{bare}(p)]. \tag{5.8}$$

The inverse propagator is given by

$$\begin{aligned} (S^{bare})^{-1}(p) &= \frac{1}{-i\not{\mathcal{C}}(p) + \mathcal{B}(p)} \\ &= \frac{i\not{\mathcal{C}}(p) + \mathcal{B}(p)}{\sum_\mu \mathcal{C}_\mu(p)^2 + \mathcal{B}^2(p)} \\ &= \frac{i\not{\mathcal{C}}(p) + \mathcal{B}(p)}{\mathcal{C}(p)^2 + \mathcal{B}^2(p)}. \end{aligned} \tag{5.9}$$

By comparing this to the continuum tree-level quark propagator, we can associate it to the mass and renormalization functions. The tree-level continuum propagator is given by

$$S^0(p) = \frac{1}{i\not{p} + m^0}. \tag{5.10}$$

When the gluon field is present, the lattice the quark propagator will have as its general form

$$S_{bare}(p) = \frac{Z(p)}{i\not{q} + M(p)}, \tag{5.11}$$

which can be defined as having inverse

$$(S^{bare})^{-1}(p) = i\sum_\mu (C_\mu(p)\gamma_\mu) + B(p). \tag{5.12}$$

Comparing with eq. (5.8) and eq. (5.7), we find

$$\begin{aligned} C_\mu(p) &= \frac{\mathcal{C}_\mu(p)}{\mathcal{C}(p)^2 + \mathcal{B}^2(p)} \\ B(p) &= \frac{\mathcal{B}(p)}{\mathcal{C}(p)^2 + \mathcal{B}^2(p)}. \end{aligned} \tag{5.13}$$

Then we define $A(p)$ by

$$S^{-1}_{bare}(p) = i\not{q}\, A(p) + B(p), \tag{5.14}$$

which can be found in terms of C_μ by

$$A(p) = \frac{q_\mu C_\mu}{q^2}. \tag{5.15}$$

Leading naturally to the definition

$$\mathcal{A}(p) = \frac{q_\mu \mathcal{C}_\mu}{q^2}. \tag{5.16}$$

Comparing to the general form of the lattice propagator, eq. (5.11), we obtain

$$\begin{aligned} Z(p) &= \frac{1}{A(p)} = \frac{\mathcal{C}^2(p) + \mathcal{B}^2(p)}{\mathcal{A}} \\ M(p) &= \frac{B(p)}{A(p)} = \frac{\mathcal{B}(p)}{\mathcal{A}(p)}. \end{aligned} \tag{5.17}$$

Noting that working with $\mathcal{A}$ and $\mathcal{B}$ rather than A and B has computational advantages, in that it allows us to use less memory by storing just those and $\mathcal{C}(p)^2 + \mathcal{B}^2(p)$.

Due to the discretisation of the derivative, we are no longer guaranteed to acquire the correct momentum with a fourier transform. Because of this, it is necessary to define the kinematic lattice momentum, q_μ using the tree level propagator, S^0 by [62]

$$(S^0)^{-1}(p) = i\not{q}\ + m^0. \tag{5.18}$$

This means it is possible to extract q_μ as $C^0_\mu(p)$. For the overlap, this simple process is the only tree-level correction necessary [65].

5.2 Results

We are now in a position to present results for the non-perturbative mass and renormalization functions, M(p) and Z(p). We choose as renormalization point $p = 4\,\mathrm{GeV}$, and average data over space-time symmetries, i.e.

$$Z^{(\mathcal{R})}(p) = \frac{Z(p)}{Z(p=4)\,\mathrm{GeV}}. \tag{5.19}$$

Errors are estimated using a second-order single-elimination jack-knife, and we perform a cylinder cut with a cutoff of $\frac{\pi}{2a}$.

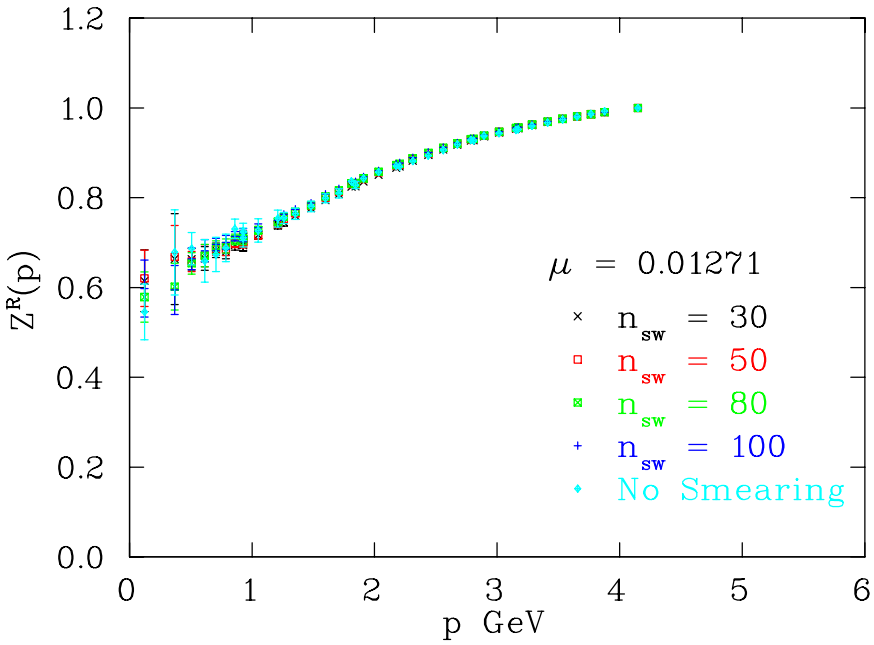

Figure 5.1: The renormalization function at $\mu = 0.01271$

Figure (5.1) shows $Z^{(\mathcal{R})}$ at the lightest quark mass considered, $m_q = 40\,\mathrm{MeV}$. This reveals the well known shape of the renormalization function dipping in the infrared region and flattening in the ultraviolet limit.

Moreover, there is little to no dependence on smearing. Of note is the comparatively large error on the two lowest momentum points. This is due to the discretisation of momentum; recall time-like momenta are discretised as

$$P_t = \frac{2\pi}{aN_t}(n + \frac{1}{2}), \tag{5.20}$$

and so we expect the smallest two points to be purely time-like. These have large errors as we have no spatial symmetries to average over, and we can expect to see the same effect for both the mass and renormalization function at all quark masses, where $Z^{(\mathcal{R})}(p)$.

Higher masses are similar, as seen in figures (5.2a-5.2l).

We now turn to the mass function. Beginning with the original, unsmeared configurations at the lightest quark mass, illustrated in figure (5.3), we note several well-known features have been reproduced here. In the infrared region we see dynamically generated mass creating a large effective quark mass. As we move to higher momenta, this drops away until an approximate plateau is seen in the ultraviolet region. Here logarithmic corrections produce the running quark mass, slightly higher than the bare quark mass, indicated by a dotted line. It is this region which we expect to be most affected by smearing, as we should have removed all gluon field physics at this range.

Examining now the lowest level of smearing on the same mass, figure (5.4), some features are immediately of note. The smeared results consistently have smaller error bars than the unsmeared, particularly in the ultraviolet region, indicating short distance physics is a significant source of noise. This can be easily understood; by smearing links we have removed much of the noise from the lattice, and so left only the fundamental non-trivial structure of the gluon field. While the instanton structure of the gauge fields varies significantly over the ensemble, their impact on the mass function remains similar across all configurations.

In the ultraviolet region, the running quark mass is now barely higher than at the input bare mass. This indicates we have spoiled the physics in this region by removing short-range effects, resulting in a quark propagator identical to the free field tree-level propagator. In the infrared region the smeared configurations have qualitatively similar behaviour to the un-

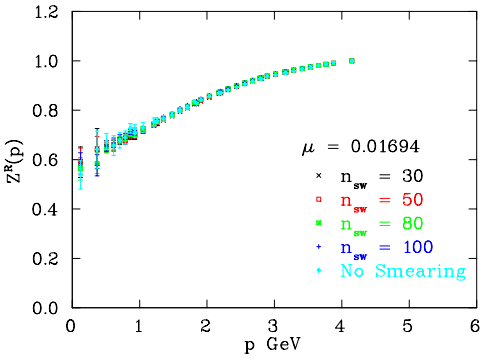

(a) Renormalization function at $\mu = 0.01694$

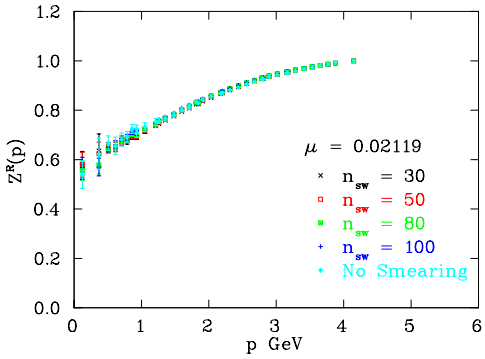

(b) Renormalization function at $\mu = 0.02119$

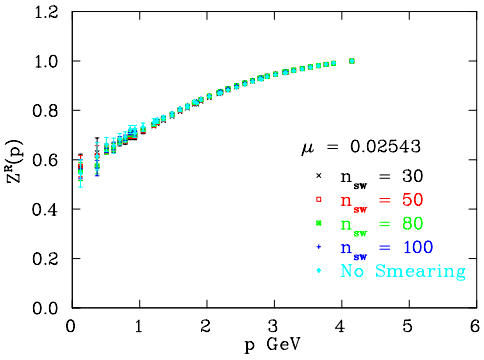

(c) Renormalization function at $\mu = 0.02543$

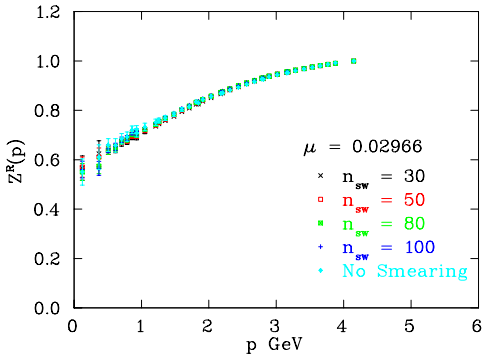

(d) Renormalization function at $\mu = 0.02966$

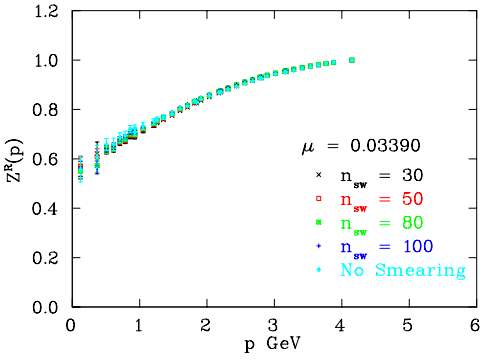

(e) Renormalization function at $\mu = 0.03390$

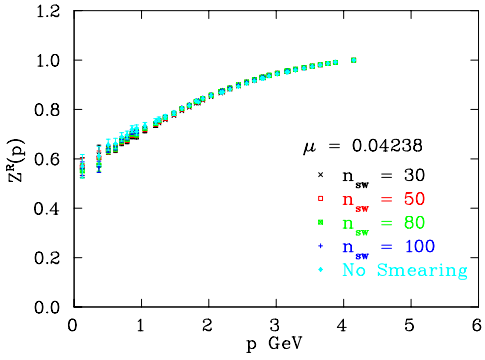

(f) Renormalization function at $\mu = 0.04238$

Figure 5.2: The renormalisation function at various values of μ

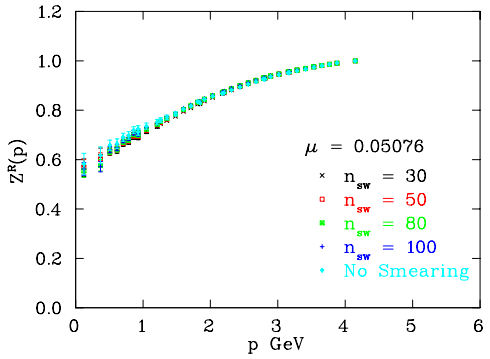

(g) Renormalization function at $\mu = 0.05076$

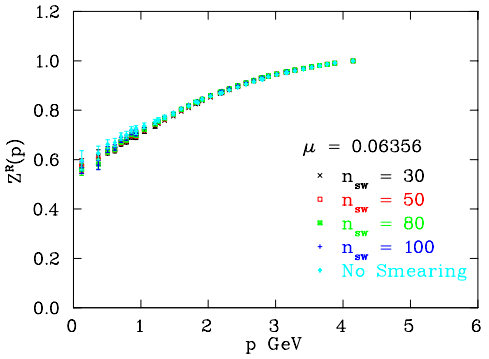

(h) Renormalization function at $\mu = 0.06356$

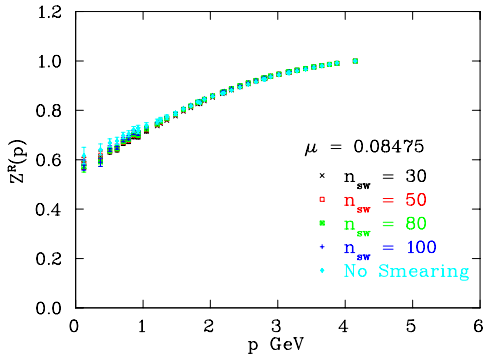

(i) Renormalization function at $\mu = 0.08475$

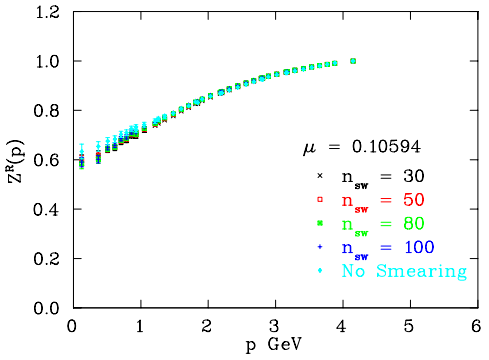

(j) Renormalization function at $\mu = 0.10594$

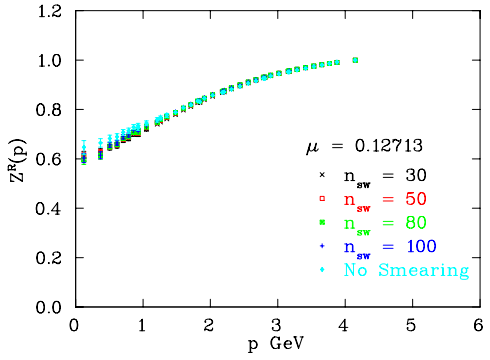

(k) Renormalization function at $\mu = 0.12713$

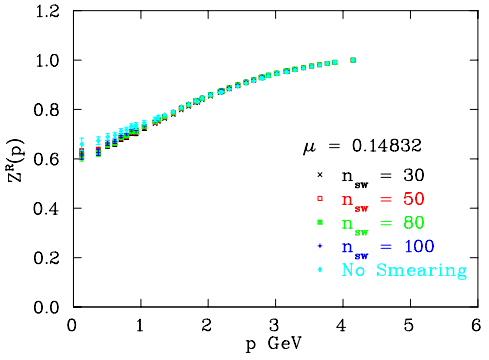

(l) Renormalization function at $\mu = 0.14832$

Figure 5.2: The renormalisation function at various values of μ

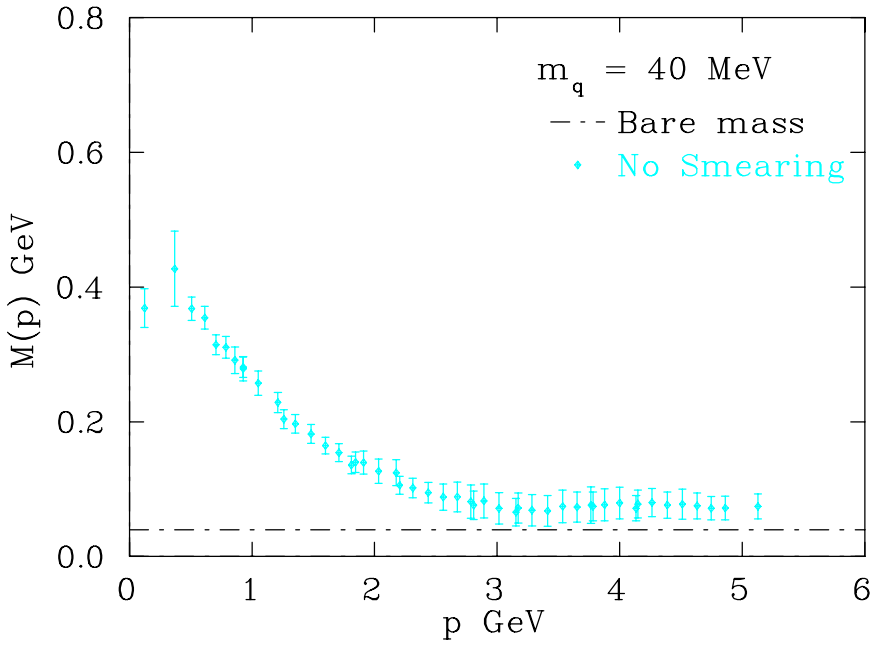

Figure 5.3: The mass function at $\mu = 0.01271$ on unsmeared configurations

smeared, featuring large mass generation. At the lowest momenta we find perfect agreement, but as we increase in momentum there is some suppression of dynamically generated mass. We attribute this to the destruction of some topological objects by the smearing algorithm, which allows instanton/anti-instanton annihilation. We also note that smearing enlarges the average radius of lattice instantons, while destroying the smallest objects.

Incorporating the next level of smearing, 50 sweeps, in figure (5.5), we see very similar results. We again have a mass plateaued on the input bare mass in the ultra violet region, although we note that at 50 sweeps the mass function remains flat at lower momenta. This is in accord with the idea that the smearing radius, the distance within which physics is suppressed, is larger. There is some reduction in dynamically generated mass in the infrared region, although the gap is not nearly as significant as between unsmeared

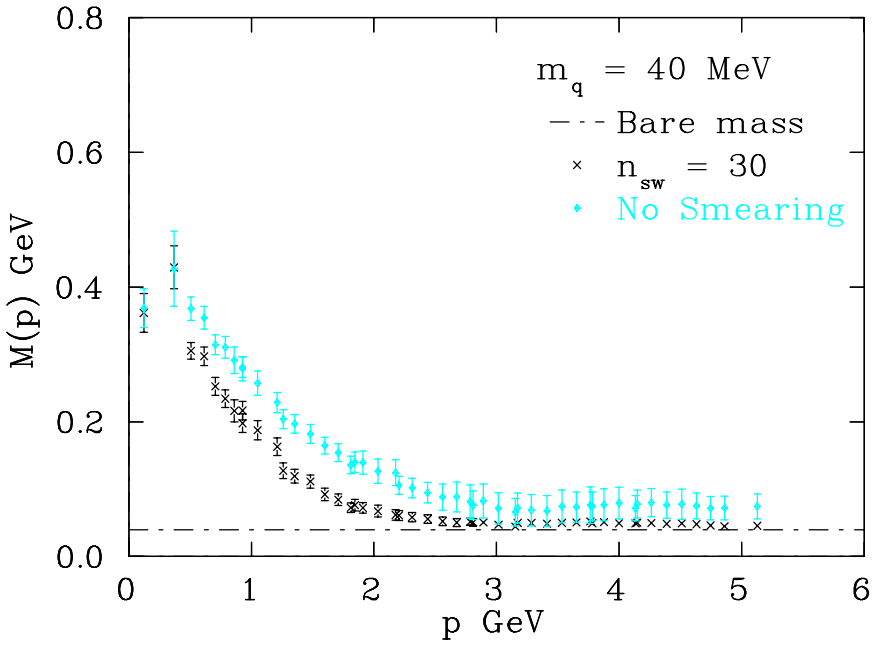

Figure 5.4: The mass function at $\mu = 0.01271$ on unsmeared configurations and 30 sweeps of smearing

configurations and 30 sweeps of smearing. This suggests that, to at least some extent, smearing has resulted in a different mass renormalization, and so in order to acquire results with the same physical mass we must shift our value of μ for the smeared results.

Before showing a plot of shifted μ, we first plot the remaining levels of smearing in figure (5.6). These continue the trends seen earlier; they remain at the input bare mass for progressively lower momenta, as well as having smaller amounts of dynamically generated quark mass. This suggests the danger of spoiling the topological structure of the vacuum by excess smearing is very real; even in the infrared region we have statistically significant reduction of dynamical mass generation at 100 sweeps of smearing, suggesting that even large instanton/anti-instanton pairs annihilate, suppressing

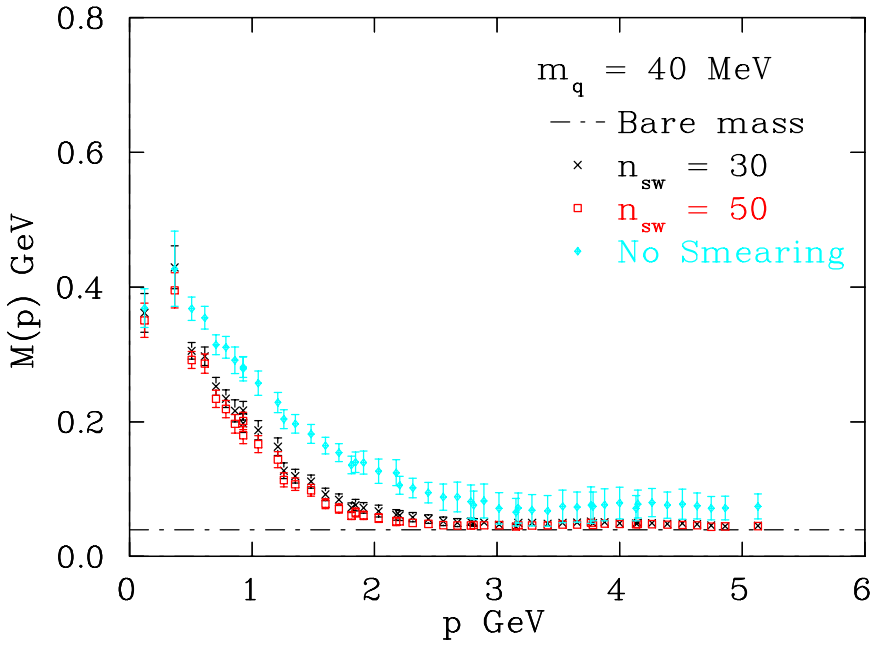

Figure 5.5: The mass function at $\mu = 0.01271$ on unsmeared configurations, and with 30 and 50 sweeps of smearing

topological effects. We do however, maintain a good qualitative shape of the curve for even the highest level of smearing considered, suggesting again that the crucial determinant of the quark propagator is the vacuum topology.

Figure (5.7) plots the smeared results at a higher value of $\mu = 0.02119$, corresponding to a bare mass of $m_q = 66\,\mathrm{MeV}$, chosen for agreement with our unsmeared results in the ultraviolet region. This shows that we cannot attribute all loss of dynamically generated mass at medium momentum ranges to changes in mass renormalization; it is clear that we have lost some important aspects of vacuum structure even after 30 sweeps of smearing. We have then plotted results for higher masses in figures (5.8a-5.8l). These show very similar results at low quark masses up to around $\mu = 0.05076\,(m_q = 159\,\mathrm{GeV})$. We do see a slight increase in the loss of dy-

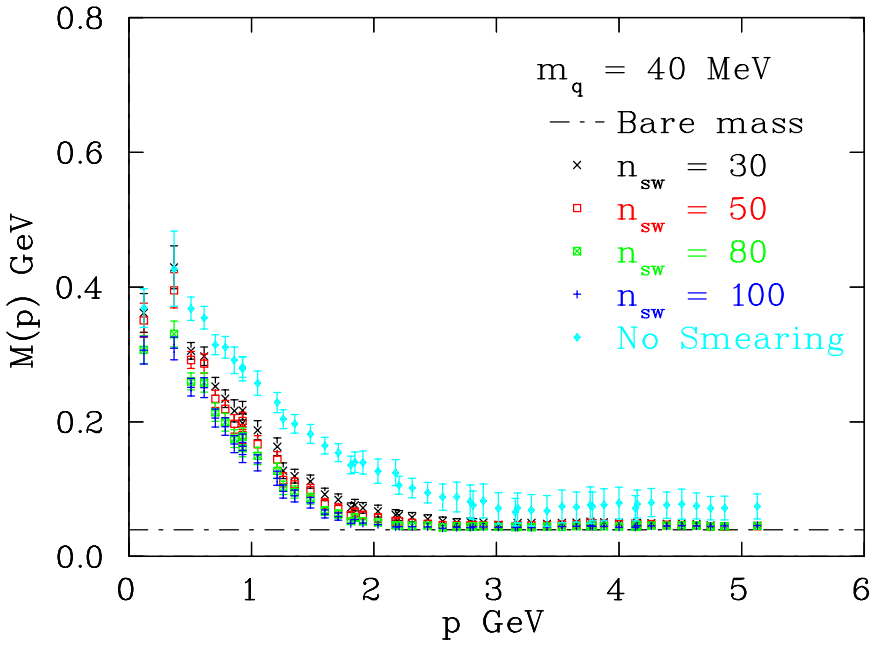

Figure 5.6: The mass function at $\mu = 0.01271$ on unsmeared configurations, 30, 50, 80 and 100 sweeps of smearing

namical mass generation at higher masses, notably between the unsmeared and 30 sweeps case. This appears to indicate the most important step is smearing to 30 sweeps, where the smallest non-trivial instanton-like objects are lost; beyond this loss of dynamical mass generation per sweep is greatly reduced. Here instanton/anti-instanton annihilation is key. We do, however see at large quark masses ($\mu > 0.05$) the smeared results behaving unusually in the ultraviolet limit, with a non-trivial running quark mass. This is most likely a result of the well-known problems with modeling heavy quark masses on the lattice, with discretisation effects expected to be most significant in the ultraviolet limit.

Altogether, we have successfully retained the important features of the quark propagator, under extensive smearing. This suggests that instantons

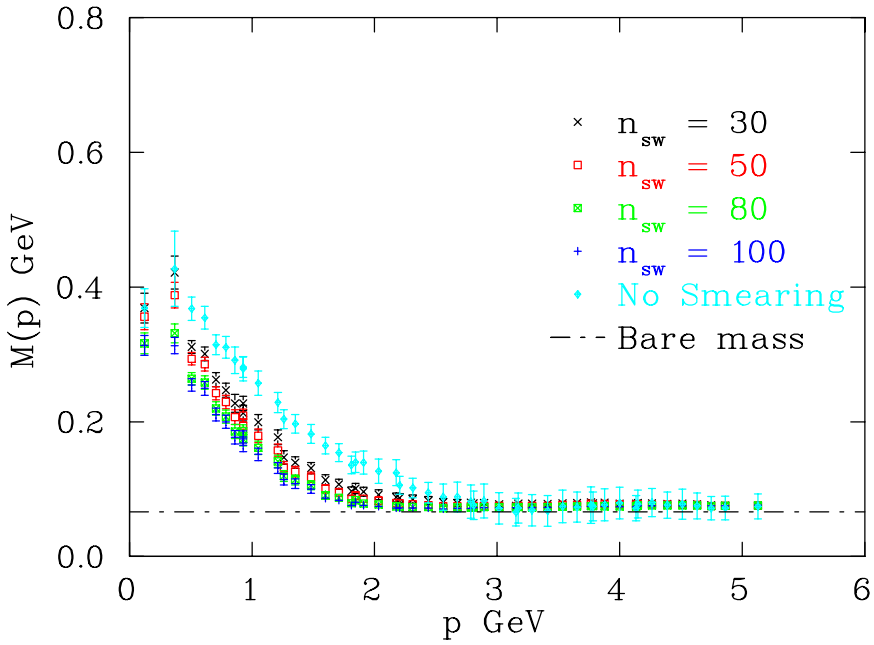

Figure 5.7: The mass function at $\mu = 0.01271$ on unsmeared configurations and at $\mu = 0.02119$ with 30, 50, 80 and 100 sweeps of smearing

play the vital role in the dynamical generation of quark mass. Indeed, they provide the majority of the physics behind the non-perturbative quark propagator, and are thus important components of the QCD vacuum.

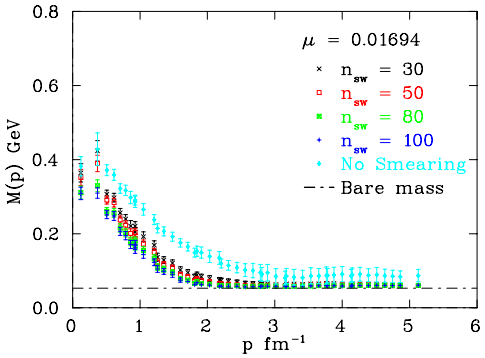

(a) Mass function at $\mu = 0.01694$

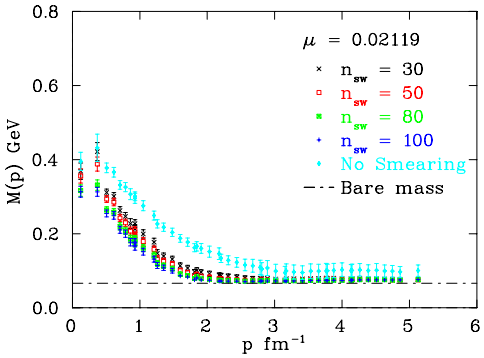

(b) Mass function at $\mu = 0.02119$

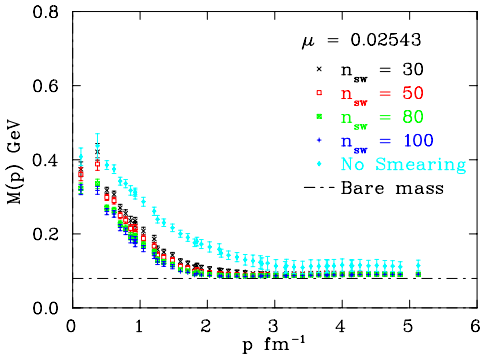

(c) Mass function at $\mu = 0.02543$

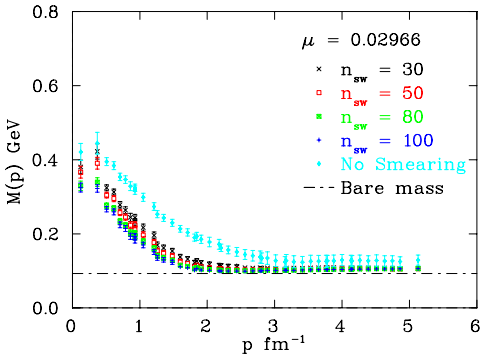

(d) Mass function at $\mu = 0.02966$

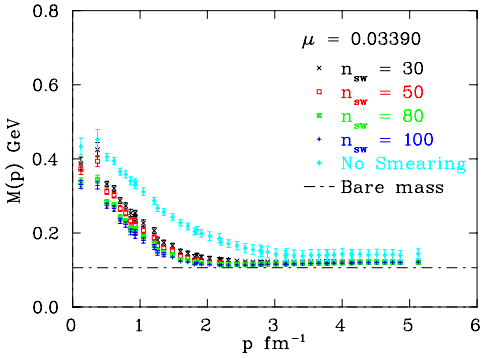

(e) Mass function at $\mu = 0.03390$

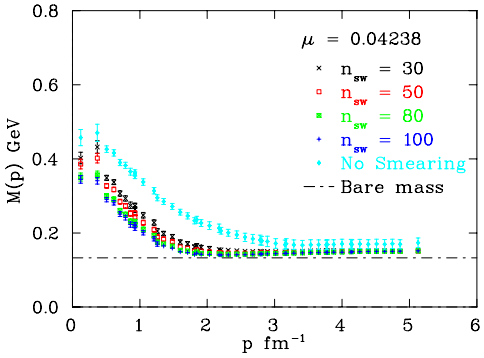

(f) Mass function at $\mu = 0.04238$

Figure 5.8: The mass function at various values of μ

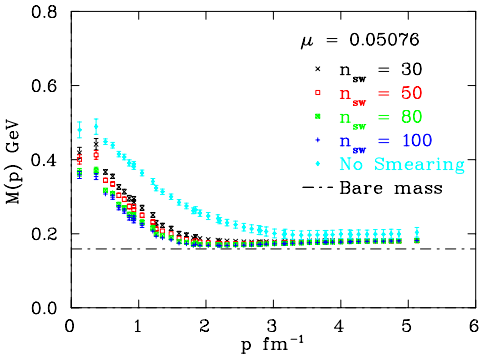

(g) Mass function at $\mu = 0.05076$

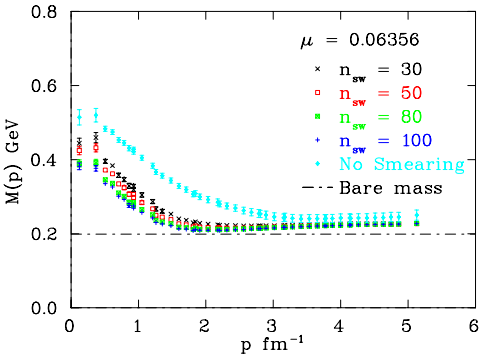

(h) Mass function at $\mu = 0.06356$

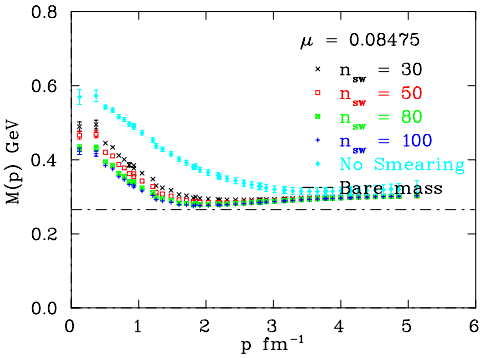

(i) Mass function at $\mu = 0.08475$

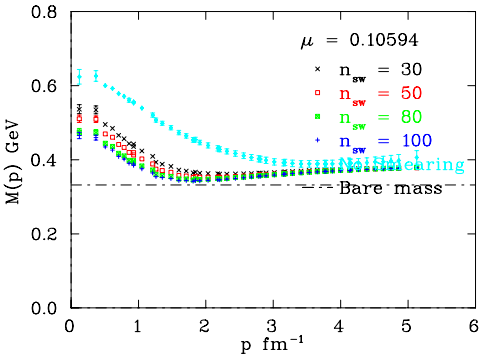

(j) Mass function at $\mu = 0.10594$

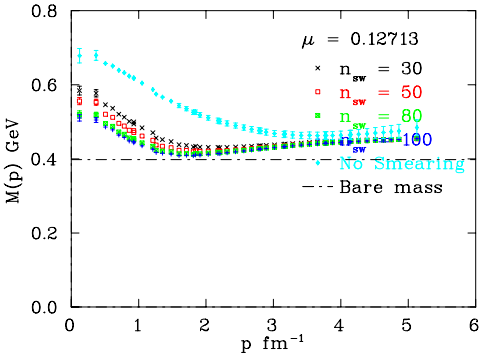

(k) Mass function at $\mu = 0.12713$

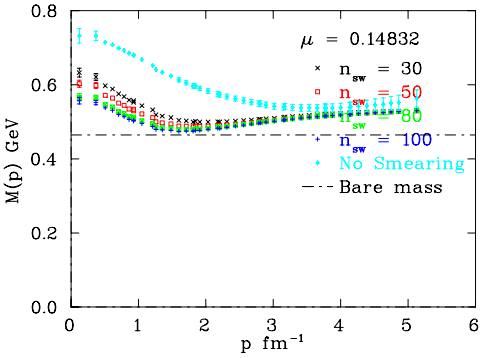

(l) Mass function at $\mu = 0.14832$

Figure 5.8: The mass function at various values of μ

Chapter 6

Conclusion

We have used over-improved stout link smearing, a form of gluonic smearing tuned to preserve instantons, as a tool to investigate the topological content of lattice gauge field configurations. By fitting the classical instanton action to the lattice, we have found the presence of topological objects which closely resemble instantons in topological charge density and structure. Using smearing removes short-range effects from the configurations as well as small topologically non-trivial aspects of the vacuum. By repeating the analysis we found that it leaves the long-range structure mostly intact. We observed that excessive amounts of smearing could enlarge the instanton-like objects, while some were also removed through annihilation in the smearing process. This gave us an optimal level of smearing of around 80 sweeps, which produced configurations with instantons closely resembling their classical counterparts, while removing all UV noise. We found that qualitatively these configurations closely resembled the well-known instanton liquid model of the QCD vacuum, while having a denser packing of larger instantons.

We then calculated the quark propagator using the overlap action, a fermion action which maintains a lattice-deformed version of chiral symmetry and thus removes additive mass renormalisation. We were then able to isolate instanton effects by calculating the non-perturbative mass and renormalisation functions on configurations with various levels of smearing and comparing to unsmeared configurations. We have found the renormalisation function is almost independent of smearing. We have found a mass func-

tion which at even low levels of smearing is identical to the bare tree-level quark mass at high momentum, suggesting we have completely removed all short range features. At low momentum, our smeared configurations are very similar to the unsmeared, reproducing the majority of the dynamical mass generation seen originally. There is some loss of mass generation, which we attribute to the removal of instantons by the smearing process, the smallest in the first sweeps of smearing and the larger later through pair annihilation. Our results suggest that instantons are responsible for almost all dynamical mass generation, and a vacuum composed entirely of them can accurately describe the long-range behaviour of the quark propagator.

The role of instantons in giving rise to the properties of hadronic matter remains to be investigated, and would constitute a natural continuation of this work.

Bibliography

[1] K.G. Wilson, Phys. Rev. D **10**, 2445 (1974)

[2] K. Symanzik, Nucl. Phys. B **226**, 187 (1983)

[3] P.O. Bowman, *On Improvement in the Study of the Lattice Gluon Propagagtor*, PhD Thesis, University of Adelaide, 2000

[4] G.P. Lepage and P.B. MacKenzie, Phys. Rev. D **48**, 2250 (1993)

[5] C. Gattringer and C.B. Lang, *Quantum Chromodynamics on the Lattice: An Introductory Presentation*, Lect. Notes Phys. 788 (Springer, Berlin Heidelberg 2010)

[6] S. Bilson-Thompson *et al*, arxiv:hep-lat/0112034

[7] M. Campostrini, A. Di Giacomo, H. Panagopoulos and E. Vicari, Nucl. Phys. B **329**, 683 (1990)

[8] D.J.R. Pugh and M. Teper, Phys. Lett. B **224**, 159 (1989)

[9] M.E. Peskin and D.V. Schroeder, *An Introduction to Quantum Field Theory* (Addison-Wesley, Reading 1995)

[10] H.J. Rother, *Lattice Gauge Theories: An Introduction* (World Scientific, Singapore 1992)

[11] T.Schäfer and E.V. Shuryak, Rev. Mod. Phys. **70**. 323 (1998)

[12] A.A. Belavin, A.M. Polyakov, A.S. Schwartz and Y.S. Tyupkin, Phys. Lett. B **59**, 85 (1975)

[13] G. 't Hooft, Phys. Rev. Lett. **37**, 8 (1976)

[14] G. 't Hooft, Phys. Rev. D **14**, 3432 (1976)

[15] M. Teper, Phys. Lett. B **162**, 357 (1985)

[16] M.F. Atiyah, N.J. Hitchin, V.G. Drinfield and Y.I. Manin, Phys. Lett. A **65**, 185 (1978)

[17] T. Banks and A. Casher, Nucl. Phys. B **169**, 103 (1980)

[18] E.V. Shuryak, Nucl. Phys. B **214**, 237 (1983)

[19] P.J. Moran, *Impact of Dynamical Fermions on the Vacuum of Quantum Chromodynamics*, PhD thesis, University of Adelaide, 2010

[20] S. Weinberg, Phys. Rev. D **11**, 3583 (1975)

[21] C.G. Callan, R.Dashen and D.J. Gross Phys. Rev. D **17**, 2717 (1978)

[22] E.V. Shuryak, Nucl. Phys. B **203**, 93 (1982)

[23] E.V. Shuryak, Nucl. Phys. B **203**, 116 (1982)

[24] E.V. Shuryak, Nucl. Phys. B **203**, 140 (1982)

[25] M. Giordano and E. Meggiolaro Phys. Rev. D **81**, 074022 (2010)

[26] E.M. Ilgenfritz, M.L. Laursen, M. Müller-Preußker, G, Schierholz and H.Schiller Nucl. Phys. B **268**, 693-705 (1986)

[27] B. Berg, Phys. Lett. B **104**, 475 (1981)

[28] Y. Iwasaki and T. Yoshié, Phys. Lett. B **127**, 259 (1983)

[29] M. Garcia Perez, A. Gonzalez-Arroyo, J. Snippe and P. van Baal, Nucl. Phys. B **413**, 453 (1994)

[30] M. Falcioni et al., Nucl. Phys. B **251**, 624 (1985)

[31] C. Morningstar and M. Peardon, Phys. Rev. D **69** (2004)

[32] A. Hasenfratz and F. Knechtli, Phys. Rev. D **64** (2001)

[33] F. Bruckmann, F. Gruber, C. B. Lang, M. Limmer, T. Maurer, A. Schfer and S. Solbrig, arxiv:0901.2286v1 (2009)

[34] P.J. Moran and D.B. Leinweber, arxiv:0801.1165v1 [hep-lat] (2008)

[35] S.O. Bilson-Thompson, F.D.R Bonnet, D.B. Leinweber and A.G. Williams, Nucl. Phys. Proc. Suppl. **109A**, 116 (2002)

[36] P.J Moran and D.B. Leinweber, Phys. Rev. D **78** (2008)

[37] I. Horvath, S.J. Dong, T. Draper, N. Isgur, F.X. Lee, K.F. Liu, J. McCune, H.B. Thacker and J.B. Zhang, Phys. Rev. D. **66**, 2002

[38] W. Kamleh, *Lattice Quantum Chromodynamics with FLIC Overlap Fermions*, PhD Thesis, University of Adelaide, 2004

[39] K. G. Wilson, CLNS-321, New Phenomena in Subnuclear Physics. Part A. Proceedings of the First Half of the 1975 International School of Subnuclear Physics, Erice, Sicily, July 11 - August 1, 1975, Plenum Press, New York, 1977, p.69

[40] J.M. Zanotti, D.B. Leinweber, W. Melnitchouk, A.G. Williams and J.B. Zhang, Lect. Notes Phys **663**, 2005

[41] H.B. Nielsen and M. Ninomiya, Nucl. Phys. B**185**, 1981

[42] H.B. Nielsen and M. Ninomiya, Nucl. Phys. B**193**, 1981

[43] H.B. Nielsen and M. Ninomiya, Phys. Lett. B**105**, 1981

[44] T. DeGrand and C. DeTar Lattice Methods for Quantum Chromodynamics, World Scientific Publishing, 2006

[45] P.H. Ginsparg and K.G. Wilson, Phys. Rev. D**25** 1981

[46] M. Lüscher, arxiv:hep-lat/9802011

[47] P.Hasenfratz, arxiv:hep-lat/9802007

[48] R. Narayanan and H. Neuberger, arxiv:hep-th/9411108

[49] H. Neuberger, arxiv:hep-lat/9910040v1

[50] H. Neuberger, Phys. Rev. D**61**, 2000 hep-lat/9911004.

[51] H. Neuberger, Phys. Rev. Lett **81** 1998

[52] H. Neuberger, Phys. Lett. B**417**, 1998. 141

[53] R.G. Edwards, U.M. Heller and R. Narayanan, arxiv:hep-lat/9905028v1

[54] B. Jegerlehner, arxiv:hep-lat/9612014

[55] E. Ya. Remez, General Computational Methods of Chebyshev Approximations, U.S. Atomic Energy Commission, 1962

[56] T. DeGrand and A. Hasenfratz, arxiv:hep-lat/0012021v1

[57] D-J. Kusterer, J. Hedditch, W. Kamleh, D.B. Leinweber and A.G. Williams, arxiv:hep-lat/011029v3

[58] W. Kamleh, D. Adams, D.B. Leinweber and A.G. Williams hep-lat/0112042v1

[59] W. Kamleh, D.J. Kusterer, D.B. Leinweber and A.G. Williams Nucl. Phys. Proc. Supp. B**119**, 2003

[60] W. Kamleh, D.B. Leinweber, A.G. Williams and J-B. Zhang arxiv:hep-lat/0209155v1

[61] W. Kamleh, P.O. Bowman, D.B. Leinweber, A.G. Williams and J-B. Zhang Nucl. Phys. Proc. Supp. B**141**. 2005

[62] W. Kamleh, P.O. Bowman, D.B. Leinweber, A.G. Williams and J-B. Zhang Phys. Rev. D**71**,2005

[63] T.-W. Chiu, T.-H. Hsieh, C.-H. Huang, and T.-R. Huang Phys. Rev. D**66** 2002, hep-lat/0206007.

[64] W. Kamleh, P.O. Bowman, D.B. Leinweber, A.G. Williams and J-B. Zhang arxiv:hep-lat/0412022v1

[65] F.D.R. Bonnet, P.O. Bowman, D.B. Leinweber, A.G. Williams and J-B. Zhang Phys. Rev. D**65**, 2002

[66] B. Sheikholeslami and R. Wohlert, Nucl. Phys. B**259**, 1985

[67] J.M. Zanotti, S. Bilson-Thompson, F.D.R. Bonnet, P.D. Coddington, D.B. Leinweber, A.G. Williams and J-B. Zhang, arxiv:hep-lat/0110216

[68] D.B. Leinweber, J.I. Skullerud, A.G. Williams and C.Parinello, Phys. Rev. D **58**, (1998)